Chromatin enhancer activity of IκBα mediates the exit from naïve pluripotency

Luis G. Palma[1,2,3,δ], Daniel Álvarez-Villanueva[1,3,4,δ], María Maqueda[1,2,3], Mercedes Barrero[5], Arnau Iglesias[1,2,3], Joan Bertran[6], Damiana Álvarez-Errico[2], Carlos A. García-Prieto[2], Cecilia Ballaré[5], Virginia Rodriguez-Cortez[2], Clara Bueno[2], August Vidal[4], Alberto Villanueva[7], Pablo Menéndez[2,3,8,9,10], Gregoire Stik[2], Luciano Di Croce[5,10,11], Bernhard Payer[5,11], Manel Esteller[2,3,10,12], Lluís Espinosa[1,3,*] & Anna Bigas[1,2,3,*]

[1]Program in Cancer Research. Hospital del Mar Research Institute, Barcelona, Spain.

[2]Josep Carreras Leukemia Research Institute, Barcelona Spain.

[3]Centro de Investigación Biomédica en Red Cancer (CIBERONC), Madrid, Spain.

[4]Institut Investigació Biomèdica de Bellvitge (IDIBELL), L'Hospitalet de Llobregat, Barcelona, Spain.

[5]Centre for Genomic Regulation (CRG), The Barcelona Institute of Science and Technology, Barcelona, Spain.

[6]Faculty of Sciences, Technology and Engineering, Universitat de Vic - Universitat Central de Catalunya, Vic 08500 Spain

[7]Chemoresistance and Predictive Factors Group, Program Against Cancer Therapeutic Resistance (ProCURE), Catalan Institute of Oncology (ICO), Oncobell Program, Bellvitge Biomedical Research Institute (IDIBELL), L'Hospitalet de Llobregat, Barcelona, Spain.

[8]Spanish Network for Advanced Therapies (RICORS-TERAV). Carlos III Health Institute (ISCIII), Spain.

[9]Department of Biomedicine. University of Barcelona, Spain.

[10]Institucio Catalana de Recerca i Estudis Avançats (ICREA), Barcelona, Spain.

[11] Universitat Pompeu Fabra, Barcelona, Spain.

[12]Physiological Sciences Department, School of Medicine and Health Sciences, University of Barcelona (UB), Barcelona, Catalonia, Spain.

[δ]These authors contributed equally

Keywords: IκBα, NFKBIA, NF-κB, DNA Methylation, Polycomb, Embryonic Stem Cells, Pluripotency Exit, Germ Layer Specification,

*Corresponding authors:

Anna Bigas and Lluis Espinosa

Cancer Research Program. CIBERONC.

Hospital del Mar Research Institute

Doctor Aiguader 88, 08003, Spain.

Tel: +34 933160440; email: abigas@researchmar.net; lespinosa@researchmar.net

Running title: IκBα function in pluripotency exit

Keywords: Embryonic Stem Cells, IkappaB, NfkappaB, Chromatin Regulation, Enhancer, Inflammation, Naïve pluripotency, Pluripotency

Abstract

Inflammation is crucial in development and cell differentiation, albeit their involvement in the transition from naïve to primed pluripotency remains elusive. One of the main sensors of inflammation is IκBα, which exerts its function through activation of NF-κB. Our previous work identified a chromatin role of IκBα that is crucial for the proper regulation of adult stem cells. Here, we demonstrate that IκBα depletion causes profound epigenetic rewiring in pluripotent stem cells characterized by altered histone post-translational modifications and DNA methylation, which is associated with changes in transcriptional regulation. These changes led to stabilization of cells in a ground state of naïve pluripotency when cultured in Serum/LIF conditions and differentiation impairment. Mechanistically, IκBα binds to intergenic chromatin regions in the naïve pluripotency state, which result in altered activation status of a subset of enhancers, including several associated to pluripotency-related genes. Through the engineering of separation-of-function mutants, we demonstrate that the effects of IκBα in the regulation of stem cell pluripotency are NF-κB-independent, but mainly relies on its chromatin-related function. Altogether, our results highlight a novel mechanism by which IκBα participates in regulating the pluripotent states of embryonic stem cells, shedding light on the interplay between inflammatory signals and pluripotency regulation.

INTRODUCTION

Embryonic Stem Cells (ESCs) pluripotency is characterized by the capacity to generate all somatic and germline lineages both *in vitro* and *in vivo*, depending on the culture conditions. When cultured in serum plus Leukemia Inhibitory Factor (LIF) (Serum/LIF), murine ESCs (mESCs) include cells interconverting to different metastable states (Festuccia et al. 2013) that either resemble preimplantation blastocyst (naïve pluripotency) or post-implantation (primed pluripotency) embryonic stages (Graf and Stadtfeld 2008; Martinez Arias and Brickman 2011; Pera and Rossant 2021; Wang and Wu 2022). The heterogeneity of mESCs in Serum/LIF is reduced by culturing them in the presence of GSK3β and MEK1/2 inhibitors (CHIR99021 and PD0325901, respectively) along with LIF (2i/LIF). Under these conditions, mESCs enter a ground state of naïve pluripotency characterized by self-renewal activity while suppressing any pro-differentiating signals (Ying et al. 2008; Marks et al. 2012). This pluripotent state closely resembles the inner cell mass of the E4.0 mouse preimplantation blastocyst (Boroviak et al. 2015). After implantation, pluripotent capability of the mouse embryo (E5.5) becomes restricted to Epiblast Stem Cells (EpiSCs), which represent a primed pluripotent state, characterized by coexpression of pluripotency and lineage specification markers (Brons et al. 2007; Tesar et al. 2007). EpiSCs can give rise to cells of the three different germ layers (endoderm, mesoderm and ectoderm), albeit their contribution to chimeras or to germ cells is greatly compromised (Weinberger et al. 2016; Pera and Rossant 2021). EpiSCs can be derived *in vitro* from naïve pluripotent cells cultured in a medium supplemented with Nodal and fibroblast growth factor (FGF) (Guo et al. 2009). Different epigenetic features distinguish naïve from primed pluripotent states (Takahashi et al. 2018), such as changes in the X chromosome inactivation in female cells (Bao et al. 2009; Guo et al. 2009), histone post-translational modifications (Tesar et al. 2007) or a global DNA hypomethylation profile observed in naïve pluripotent stem cells (Habibi et al. 2013; Leitch et al. 2013; Singer et al. 2014). These epigenetic changes are a prerequisite for the subsequent activation of gene circuits associated with pluripotency exit and germ layer specification (Brons et al. 2007; Tesar et al. 2007). Crucial regulatory elements for the transition from naïve to primed pluripotency state are located in distal DNA regions or enhancers to facilitate the resolution toward the primed state (Factor et al. 2014; Buecker et al. 2014). Therefore, identifying novel players to fine-tune the equilibrium between ground and primed states is crucial for preserving both pluripotency stability and differentiation capability in mESCs.

Inflammation is a defense mechanism mostly activated in response to harmful endogenous or foreign stimuli, which involves different signaling pathways including NF-κB. Canonical NF-κB signaling is triggered by the IKK kinase complex, which induce the phosphorylation and subsequent degradation of the NF-κB inhibitor, IκBα, leading to nuclear translocation of the NF-κB factors (e.g. p50/p65) (Zhang et al. 2017). We have previously identified an alternative nuclear function of IκBα involving the interaction with histone deacetylases (HDACs), core elements of the Polycomb Repressor Complex 2 (PRC2) and histones (Aguilera et al. 2004;

Mulero et al. 2013; Marruecos et al. 2021). This nuclear IκBα function is crucial for tissue stem cell homeostasis and the proper differentiation of epidermal, intestinal and hematopoietic cells (Mulero et al. 2013; Marruecos et al. 2020, 2021; Thambyrajah et al. 2022).

There is now robust evidence that inflammatory signals are crucial in stem cell development (Gerondakis et al. 2006; Kaltschmidt et al. 2021), and it was recently demonstrated that attenuation of inflammatory signals by ATG5 facilitates mESCs differentiation (Li et al. 2024). Unexpectedly, being NF-κB pathway a pivotal regulator of inflammation, classical NF-κB factors including p50 and RelA/p65 are expressed at very low levels in mESCs. Overexpression of NF-κB proteins leads to cell differentiation while expression of the IκBα super-repressor (S32-36A mutant) increases expression of pluripotency markers (Torres and Watt 2008). Similarly, inhibition of Protein Kinase C (PKC) activity in mESCs, which in turn restrains NF-κB signaling, allows keeping mESCs in a ground pluripotency state, thus facilitating the generation of induced pluripotent stem cells (iPSCs) (Dutta et al. 2011). Together these results indicate that NF-κB inhibition is required for maintaining the pluripotent state of murine ESCs. Given the importance of NF-κB in the multiple aspects of stem cell biology (Espín-Palazón and Traver 2016) and the pivotal role of IκBα in NF-κB regulation, the possible impact of the IκBα chromatin function in cell fate has remained challenging.

We have now investigated the role of IκBα in a context of pluripotent stem cells. Unexpectedly, and in contrast with the pro-differentiation effects of NF-κB activation, depletion of the NF-κB inhibitor IκBα precludes the exit of mESCs from naïve pluripotency associated with an epigenetic rewiring. By using the recently described Separation-Of-Function (SOF) IκBα mutants (Alvarez-Villanueva et al. 2023), we have now demonstrated that pluripotency regulation by IκBα is mainly exerted through its chromatin-related function but independent on its capacity to negatively regulate NF-κB.

RESULTS

IκBα accumulates in the chromatin of naïve pluripotent cells

Because of the prominent role of NF-κB signaling in mESCs regulation, we analyzed the expression pattern of the different NF-κB members including the IκB inhibitors in the three defined pluripotent stages: ground state of naïve pluripotency (2i/LIF), naïve pluripotency (Serum/LIF), and primed pluripotency (Epiblast Stem Cells or EpiSCs) (Figure 1A). In agreement with NF-κB being a pro-differentiation factor, canonical NF-κB inhibitors including IκBα (*Nfkbia*), IκBβ (*Nfkbib*) and IκBε (*Nfkbie*) were all expressed in the naïve pluripotency state (both ground and Serum/LIF), with *Nfkbia* levels significantly reduced upon naïve pluripotency exit towards EpiSCs (Figure 1B). In contrast, *Rela, Nfkb1 and Nfkb2 genes* codifying for the NF-κB factors p65/RelA, p105 and p100, respectively, showed an opposite pattern and either increased or maintained their levels in EpiSCs (Figure 1C). We further characterized the distribution of IκBα in the cytoplasm, nucleus and chromatin fractions of the three states of pluripotency (Figure 1D). IκBα protein levels in the cytoplasm and the nucleus correlated with the detected RNA levels in the three different cellular states being highest in 2i/LIF condition (Figure 1B). Interestingly, a notable accumulation of IκBα was observed in the chromatin of naïve pluripotent cells cultured in Serum/LIF conditions compared to 2i/LIF. In contrast, IκBα was entirely absent from the chromatin of EpiSCs. (Figure 1D). The abundance of IκBα RNA and protein in the context of naïve pluripotency compared to EpiSCs was further corroborated through analysis of an additional database encompassing both naïve and primed pluripotent states (Atlasi et al. 2020) (Figure 1E).

Next, we studied IκBα expression in differentiated embryoid bodies (EBs) from mESCs (Serum/LIF) (see materials and methods) and analyzed the expression levels of different pluripotency (*Dppa4, Pou5f1, Sox2, Prdm14, Klf4, Zfp42 [Rex1], Nanog*), differentiation-linked (*Mesp1, Gata6, Lhx1, Gata4, Wnt3a, Fgf5, Nes, Axin2, Wnt3, Eomes, T, Foxa2, Mixl1, Lef1*), and NF-κB genes (*Nfkbid, Nfkbia, Nfkbie, Nfkbib, Nfkbiz, Rel, Rela, Relb*) by RNA sequencing. *Nfkbia* (IκBα gene) was expressed at higher levels specifically in mESCs (Serum/LIF) whereas cells undergoing differentiation (48h and 96h) displayed a reduction in its expression levels (Figure 1F). The expression pattern of *Nfkbia* was similar to the pluripotency genes, whereas most of the NF-κB genes were upregulated upon differentiation, clustering together with developmental genes, as previously described (Torres and Watt 2008).

Taken together, these data show that the expression of *Nfkbia*, like the other *Nfkbi*, is high in the naive pluripotent state, in contrast to the NF-κB genes, which cluster together with differentiation markers. In addition, IκBα accumulates in the chromatin of naive pluripotent cells, more so in cells cultured under serum/LIF.

Lack of IκBα impairs the exit from the naïve pluripotency state

To investigate the functional implication of the chromatin accumulation of IκBα in naïve pluripotency, we knocked-out IκBα protein in mESCs by CRISPR-Cas9 (IκBα-KO mESCs) (Figure 1G and materials and methods). We did not detect major changes in NF-κB target genes upon IκBα depletion neither in mESCs, nor 48h and 96h EBs (Figure 1H), suggesting that NF-κB regulation did not require IκBα at this stage or it might be compensated by the other canonical or non-canonical IκBs (IκBβ, IκBε or p100), as previously demonstrated (Hayden and Ghosh 2008; Basak et al. 2007). Paradoxically, IκBα-KO mESCs have an impaired capability to undergo differentiation, since IκBα-KO EBs cannot properly evolve towards differentiation trajectories (Figure 2A). This observation was confirmed by analysis of naïve pluripotency markers at 96h (*Gab1, Sox2, Esrrb, Zfp42, Dppa4, Klf2, Prdm14, Klf4, Tfcp2l1*), which displayed higher expression levels in IκBα-KO compared to their wild-type (IκBα-WT) counterparts (Figures 2B and S1A). Differentiation of IκBα-KO EBs was deficient in programs associated with all germ layer specification (endoderm, mesoderm, and ectoderm) (Figures 2C-E). Moreover, IκBα-KO EBs were smaller in size (Figure S1B), and maintained higher expression of the pluripotency program even at 216h (Figures 2F and S1C). We also detected a higher number of Alkaline Phosphatase-expressing cells (Figures 2G and S1D) and higher expression of the pluripotency marker SSEA-1 (Figure S1E) at 216h IκBα-KO EBs. To further study the requirement of IκBα in pluripotency exit *in vivo*, we established teratomas by subcutaneous injection of IκBα-WT and IκBα-KO mESCs (Figure S1F and materials and methods) in NSG (NOD.Cg-Prkdc^{scid} Il2rg^{tm1Wjl}/SzJ) mice. IκBα-KO teratomas showed a decreased differentiation potential, as indicated by higher number of OCT4^{+} cells (Figures S1G-H). These observations underscore the essential role of IκBα in the exit from the pluripotency state in mouse embryonic stem cells (mESCs).

To determine the specific time-point in which IκBα is required for pluripotency exit, we differentiated IκBα-WT and IκBα-KO mESCs cultured in Serum/LIF (naïve pluripotency) towards EpiSCs (primed pluripotency) for 120h (Figure 2H and materials and methods). IκBα-KO cells were not committed towards the primed pluripotency stage and maintained an elevated expression levels of naïve pluripotency genes (*Dppa3, Nanog, Sox2, Rex1, Klf2, Klf4, Gbx2, Tbx3*) (Figure 2I). Additionally, IκBα-KO cells retained a naïve pluripotent morphology, forming tight clusters and resembling cells cultured in 2i/LIF medium (Figure S1I). These data demonstrate that IκBα is required for the exit of the naïve state of pluripotency and its deficiency results in impaired differentiation of mESC *in vivo* and *in vitro*, without imposing major changes in the regulation of canonical NF-κB.

IκBα-KO mESCs resemble the ground-state of naïve pluripotency under Serum/LIF conditions

As mentioned, mESCs cultured in serum/LIF are highly heterogeneous, containing a mixture of cell states that resemble developmental transitions from preimplantation (naïve pluripotency) to postimplantation (primed pluripotency) embryo (Graf and Stadtfeld 2008; Martinez Arias and Brickman 2011). To investigate how IκBα deficiency was affecting the exit

193 of mESCs from naïve pluripotency, we performed a Gene Set Enrichment Analysis (GSEA)
194 using RNA-seq data from IκBα-KO and IκBα-WT mESCs cultured in Serum/LIF against gene
195 signatures for ground (2i/LIF) and naïve (Serum/LIF) pluripotency (Ghimire et al. 2018). GSEA
196 results revealed a significant enrichment in Serum/LIF IκBα-KO mESCs transcriptome for
197 genes specifically expressed in the ground state (2i/LIF), while they negatively correlate with
198 mESCs cultured in Serum/LIF (Figure 3A) (Ghimire et al. 2018). Specifically, IκBα-KO mESCs
199 expressed higher levels of the ground state pluripotency genes *Klf2, Nanog, Pou5f1, Prdm14,*
200 *Gbx2, Tbx3, Zfp42[Rex1]* and *Klf4* (Figure 3B), similar to IκBα-WT mESCs cultured in 2i/LIF
201 (Figure S2A). Since ground (2i/LIF) and naïve (Serum/LIF) states are characterized by
202 important differences in epigenetic marks, we carried out an epigenetic profiling of IκBα-WT
203 and IκBα-KO mESCs cultured in Serum/LIF. We performed chromatin immunoprecipitation
204 followed by sequencing (ChIP-seq) of histone modifications associated to gene activation
205 (H3K4me3), gene repression (H3K27me3) and constitutive heterochromatin (H3K9me3)
206 (Figures 3C-D and S2B-D). Overall, Serum/LIF IκBα-KO mESCs exhibited a more permissive
207 chromatin status as evidenced by increased H3K4me3 and decreased H3K9me3 levels, while
208 H3K27me3 was redistributed in both directions (Figure 3C). Notably, the gain in H3K4me3
209 mark was associated with a reduction of H3K27me3 levels in genes associated with naïve
210 pluripotency (Figures 3C-D and S2B-C), in agreement with the higher pluripotent state
211 observed in IκBα-KO mESCs. As mentioned, detection of the H3K9me3 mark was significantly
212 reduced in IκBα-KO mESCs (Figures 3C and S2D). These regions correspond to genes involved
213 in DNA methylation and chromatin edition functions (Figure 3C). By analyzing the DNA
214 methylation status under Serum/LIF conditions by immunofluorescence of 5-methyl-cytosine
215 (5mC) we found a global DNA hypomethylation in IκBα-KO mESCs (Figure 3E), which is one of
216 the key features of the ground state of naïve pluripotency (2i/LIF) (Habibi et al. 2013; Yagi et
217 al. 2017). To further characterize the DNA methylation status in IκBα-KO cells, we performed
218 DNA methylation arrays (Zhou et al. 2022) in IκBα-KO and IκBα-WT mESCs (Serum/LIF) and
219 96h after EB differentiation. We observed a strong reduction of the DNA methylation level in
220 IκBα-KO mESCs in a genome-wide fashion (Figure 3F). Specifically, IκBα-KO mESCs contain
221 lower DNA methylation levels in promoters, gene bodies, enhancers and imprinted regions
222 (Figure 3G), and this DNA hypomethylation status was not associated with any particular
223 chromosome (Figure S2E). DNA hypomethylation was maintained upon 96h in IκBα-KO EBs
224 (Figures 3F-G and S2F).

225 These results further indicate that IκBα is required for the transition from ground to primed
226 pluripotent states and for the proper regulation of the histone post-translational
227 modifications (PTMs) and DNA methylation changes associated with this process. We propose
228 that the enhanced pluripotent state found in IκBα-KO mESCs under basal conditions
229 (Serum/LIF) may negatively impact on their differentiation potential, similar to that described
230 for other models with stabilized naïve pluripotent state (Choi et al. 2017; Di Stefano et al.
231 2019).

232 **IκBα binds to intergenic regions to attenuate the activation status of chromatin linked to**
233 **naïve pluripotency genes**

234 To gain insight into the mechanism by which IκBα regulates the transition from naïve to
235 primed pluripotent states, we knocked-in a 3xFLAG-tag into the IκBα locus and used these
236 transgenic cells for ChIP-seq assay with the anti-FLAG antibody (see Materials and Methods).
237 We identified 817 bona-fide IκBα-bound chromatin regions which were consistent between
238 three independent replicates (Figure S3A). Among all the genome regions, IκBα was mainly
239 bound to distal intergenic and intronic regions (38.5% and 42.2% of total IκBα peaks,
240 respectively) (Figure 4A). Interestingly, IκBα-bound regions coincide with those that gain
241 enhancer activation-related H3K27Ac signals in EpiSCs (Figures S3B-C). The fact that IκBα was
242 released from chromatin at the stage of primed pluripotency (Figure 1D) suggested that IκBα
243 might be involved in fine-tuning these regions at the exit from naive pluripotency. To address
244 this question, we quantified the total amount of H3K27Ac (active enhancer) by western blot
245 analysis of chromatin extracts of IκBα-WT and IκBα-KO mESCs cultured in Serum/LIF. We
246 observed an increase of this activation mark in IκBα-KO mESCs, whereas we did not observe
247 global changes in H3K4me1 levels, a marker of poised enhancers (Figures S3D-E). These
248 results suggested that IκBα depletion in naïve pluripotency might lead to an increase in the
249 global levels of active enhancers, which are characterized by a gain of H3K27Ac without
250 changes in H3K4me1 levels (Wu et al. 2023). The increase in H3K27Ac was further validated
251 by ChIP-seq experiments conducted in both IκBα-WT and IκBα-KO mESCs. Notably, depletion
252 of IκBα protein under Serum/LIF conditions led to an increase in the deposition of H3K27Ac
253 at regions where we detected IκBα binding (Figure 4B), while levels of H3K4me1 were not
254 generally altered. Since IκBα deficiency was affecting enhancer-related histone marks, we
255 further profiled the enhancer status of IκBα-KO mESCs by analyzing the differential
256 distribution of poised enhancers (showing changes in H3K4me1 levels without affecting
257 H3K27Ac) and active enhancers (chromatin regions decorated with H3K4me1 that also display
258 H3K27ac binding) (Figures 4D). Overall, IκBα-KO mESCs showed a reduction in poised
259 enhancers at genes (or related genomic regions) associated to differentiation processes
260 (Figures 4D and S3F), whereas active enhancers of genes associated to pluripotency were
261 significantly enriched (Figures 4D-E and S3G). These results further support that mESCs lacking
262 IκBα are epigenetically reinforced in the ground state of naïve pluripotency. Since the majority
263 of IκBα chromatin peaks were located in distal intergenic and intronic regions (Figure 4A), and
264 we found that IκBα deficiency led to changes in the enhancer status (Figure 4D), we took
265 advantage of publicly available Hi-C data to identify topologically associating domains (TADs)
266 at putative IκBα target genes in Serum/LIF mESCs (Bonev et al. 2017). It was previously
267 demonstrated that TADs are organized in distinct chromatin compartments defined as active
268 (Compartment A) or inactive (Compartment B) (Lieberman-Aiden et al. 2009). Importantly,
269 chromatin regions bound by IκBα mainly correspond to TADs of the active compartment
270 (81%), whereas a small proportion of IκBα peaks were found in inactive chromatin (19%)
271 (Figure S3H). Furthermore, TADs harboring IκBα binding exhibited a greater proportion of

272 enhancers differentially regulated in IκBα-KO cells when compared to all TADs (92% vs. 74%,
273 respectively) (Figure S3H). Additionally, genes located within TADs bound by IκBα are
274 predominantly associated with mechanisms linked to pluripotency identity (data not shown).
275 To address the functional relevance of this observation, we investigated the expression
276 pattern of pluripotency-related genes in IκBα-WT and IκBα-KO mESCs at naïve pluripotency
277 (cultured in Serum/LIF) and differentiation (48h EBs) stages (Figure 4F). Most of the genes
278 analyzed were significantly upregulated in IκBα-KO mESCs, and this difference was further
279 accentuated in IκBα-KO 48h EBs. These results suggest that IκBα modulates the dynamic
280 expression of pluripotency genes through a distal regulatory mechanism involving enhancer
281 activity and 3D chromatin architecture. To address this hypothesis, we crossed Hi-C data with
282 ChIP-seq of IκBα and enhancer-related histone marks (H3K27Ac and H3K4me1), together with
283 RNA-seq data. In this meta-analysis, we identified a TAD region encompassing the Tbx3 locus
284 with IκBα binding sites (Figure 4G). Interestingly, we observed that the IκBα-bound regions
285 interact with the region containing Tbx3 gene (Figure 4G; interactions highlighted with an
286 arrow in the contact map). Moreover, that region harbors an active enhancer marked by
287 H3K27Ac/K4me1, whose activation status is heightened in IκBα-KO mESCs, likely participating
288 in increased expression of the Tbx3 gene (Figure 4G, bottom panel) and other interactions are
289 detected between the differentially activated enhancer and the Tbx3 locus in this TAD (Figure
290 4G, interaction highlighted with a gray arrow in the contact map).

291 We then determined whether differential enhancer activation status observed in IκBα-KO
292 mESCs (evidenced by increased H3K27Ac) was reversible. We engineered a doxycycline-
293 inducible IκBα construct and introduced it into IκBα-KO mESCs. Treatment of these cells with
294 doxycycline for several passages under Serum/LIF conditions (i-IκBα^{WT} mESCs, Figure 4H) led
295 to sustained IκBα expression and a significant reduction of global levels of H3K27Ac (Figures
296 4I and S3I). Ectopic expression of i-IκBα^{WT} in mESCs was also sufficient to attenuate the
297 expression of the naïve pluripotency genes *Zfp42, Klf2, Sox2* and *Tbx3 in* IκBα-KO mESCs under
298 Serum/LIF conditions (Figure S3L).

299 **IκBα attenuates the activation of intergenic regions in an NF-κB independent manner**

300 Uncovering the actual impact of chromatin-related IκBα function is challenging due to the
301 predominant role of this protein on NF-κB regulation. Recent work from our group has
302 identified the residues in the IκBα protein critical for NF-κB-binding or chromatin-binding
303 through H2A/H4. Mutation of these residues, allows to specifically discriminate between
304 either of the two functions of IκBα (Alvarez-Villanueva et al. 2023). We generated doxycycline-
305 inducible constructs to express separation-of-function (SOF) IκBα mutants: i) exclusively
306 interacts with NF-κB and is deficient for chromatin binding (i-IκBα$^{\Delta Chromatin}$) or ii) interacts with
307 histones but is deficient for NF-κB interaction and inhibition (i-IκBα$^{\Delta NF\text{-}\kappa B}$) (Figure 5A). We
308 introduced one of the SOF IκBα mutants into IκBα-KO mESCs and confirmed their functionality
309 by pull-down experiments. We found that i-IκBα$^{\Delta NF\text{-}\kappa B}$ was able to interact with histone H2A
310 but not with the NF-κB member p50 and, i-IκBα$^{\Delta Chromatin}$ could interact with p50 but not with

311 H2A, while i-IκBα^{WT} preserved all interactions (Figures 5B-C). Importantly, when we induced
312 the three different IκBα forms (i-IκBα^{WT}, i-IκBα$^{\Delta NF\text{-}\kappa B}$ and i-IκBα$^{\Delta Chromatin}$, Figure S4A), only i-
313 IκBα^{WT} and i-IκBα$^{\Delta NF\text{-}\kappa B}$ were found in the chromatin fraction of mESCs, whereas IκBα$^{\Delta Cromatin}$
314 was retained in the cytoplasm (Figures 5D and S4B). To address whether IκBα was
315 participating in the stabilization of the ground-state of naïve pluripotency in an NF-κB-
316 independent manner, we studied which of the SOF mutants (IκBα$^{\Delta NF\text{-}\kappa B}$ or IκBα$^{\Delta Chromatin}$) was
317 able to reverse the phenotype of IκBα-KO mESCs (Figure S4C). We observed the reduction of
318 the global levels of H3K27Ac upon induction of i-IκBα^{WT} and i-IκBα$^{\Delta NF\text{-}\kappa B}$, but not of
319 IκBα$^{\Delta Chromatin}$ (Figures 5E and S4D). Similarly, induction of IκBα$^{\Delta NF\text{-}\kappa B}$ was enough to reduce the
320 H3K27Ac amount in enhancers with increased H3K27Ac in IκBα-KO mESCs, but not when
321 IκBα$^{\Delta Chromatin}$ was expressed (Figure 5F). Interestingly, H3K4me1 levels followed a similar
322 pattern as H3K27Ac in those specific loci, and a significant reduction was achieved upon
323 IκBα$^{\Delta NF\text{-}\kappa B}$ overexpression, whereas IκBα$^{\Delta Chromatin}$ was mediating an opposite effect (Figure 5G).
324 In addition, the ground state-associated DNA hypomethylation was reverted in i-IκBα^{WT} and
325 i-IκBα$^{\Delta NF\text{-}\kappa B}$ mESCs but not in i-IκBα$^{\Delta Chromatin}$ mESCs (Figure 5H). Furthermore, the naïve
326 pluripotent gene expression (*Zfp42, Klf2, Sox2*, *Tbx3*) was reduced upon inducing i-IκBα$^{\Delta NF\text{-}\kappa B}$,
327 while induction of i-IκBα$^{\Delta Chromatin}$ resulted in their increase (Figure S4E).

328 To address whether reverting to the basal epigenetic status is enough to rescue the
329 differentiation capability, i-IκBα^{WT}, i-IκBα$^{\Delta NF\text{-}\kappa B}$ and i-IκBα$^{\Delta Chromatin}$ mESCs were differentiated
330 into EBs (Figure S4C). Induction of IκBα^{WT} and IκBα$^{\Delta NF\text{-}\kappa B}$ was enough to restore the
331 differentiation potential of IκBα-KO mESCs, since the number of differentiated cells (based on
332 percentage of SSEA-1^{neg} cells) increased (Figures 5I and S4F). Moreover, we found a reduced
333 number of AP+ colonies from 216h IκBα-KO EBs after induction of i-IκBα^{WT} and i-IκBα$^{\Delta NF\text{-}\kappa B}$,
334 similar to the number of colonies obtained from IκBα-WT EBs (Figures 5J and S4G). Lastly, the
335 number of remaining pluripotent-like cells (defined by OCT3/4 NANOG staining) was also
336 reduced in i-IκBα^{WT} and i-IκBα$^{\Delta NF\text{-}\kappa B}$ 216h EBs, and only small and few regions of
337 undifferentiated cells was observed (Figures 5K and S4H). On the other hand, induction of i-
338 IκBα$^{\Delta Chromatin}$ did not restore the differentiation potential of IκBα-KO mESCs, and phenocopied
339 the differentiation defects observed in IκBα-depleted mESCs.

340 These results demonstrate that the chromatin-dependent IκBα function, but not its NF-κB-
341 related activity, is necessary and sufficient to revert the stabilization in the ground state of
342 naïve pluripotency correlating with higher DNA methylation and lower H3K27Ac levels. Our
343 results demonstrate that the chromatin function of IκBα alters the activation status of
344 enhancers, which impacts the expression of genes involved in the maintenance of the naïve
345 pluripotency. This function is independent of the NF-κB-inhibitory activity of IκBα.

346 **DISCUSSION**

347 Here we have identified a new and unexpected function for the IκBα protein in the regulation
348 of the naïve pluripotency exit. Using mESCs to investigate the role of IκBα in pluripotency
349 maintenance and differentiation, we discovered that the absence of IκBα severely impairs the
350 exit of pluripotency. Furthermore, IκBα-KO mESCs stabilizes the ground state of naïve
351 pluripotency under Serum/LIF conditions, shedding light on its function as a critical regulator
352 of the transition from naïve to primed pluripotency. While IκBα is commonly known for its
353 role as an inhibitor of the NF-κB signaling pathway (Zhang et al. 2017), our laboratory has
354 previously furnished compelling evidence of its alternative role through its interaction with
355 histones and other chromatin components (Aguilera et al. 2004; Mulero et al. 2013;
356 Marruecos et al. 2021). We have demonstrated that chromatin-bound IκBα plays a crucial
357 role in regulating skin and intestinal stem cells (Mulero et al. 2013; Marruecos et al. 2020),
358 hematopoietic stem cell development (Thambyrajah et al. 2022), and it influences the
359 regenerative capacity of these tissues, and in some cases, their susceptibility to neoplastic
360 transformation. Disentangling the chromatin-related function of IκBα from its canonical role
361 as an inhibitor of NF-κB has been challenging, making it difficult to determine its truly
362 biological significance. To tackle this challenge, we engineered separation-of-function (SOF)
363 mutants of IκBα, as detailed in (Álvarez-Villanueva et al. 2023), by identifying specific residues
364 that are essential for binding either NF-κB elements or histones. Interestingly, we have shown
365 that only the histone-binding proficient IκBα mutant (IκBα$^{\Delta NF\text{-}\kappa B}$), which lacks the ability to
366 bind to NF-κB, has the capability to reverse the stabilization of the ground state observed in
367 IκBα-KO mESCs. This is sufficient to facilitate their exit from the state of naïve pluripotency,
368 restoring their full differentiation potential (Figure 5). The involvement of NF-κB in
369 pluripotency has been a subject of prior investigation. Studies have revealed that pluripotent
370 cells display a dampened inflammatory signaling pathway, which is induced upon
371 pluripotency dissolution and activation of differentiation (Torres and Watt 2008; Guo 2019).
372 However, the precise molecular mechanisms underlying the attenuated status of NF-κB
373 during this stage remain incompletely understood. A recent work has shed light on a potential
374 regulatory axis involving ATG5-β-TrCP1-NF-κB, proposing it as a mechanism that diminishes
375 NF-κB activity by stabilizing the IκBα protein in mESCs (Li et al. 2024). In any case, since
376 modification of canonical NF-κB activity directly impacts on the levels IκBα expression, the
377 previous NF-κB-associated phenotypes should be reevaluated considering this chromatin role
378 of IκBα. Furthermore, the expression of IκBα$^{\Delta Chromatin}$, which retains the inhibitory function of
379 NF-κB, failed to mitigate the ground state stabilization observed in IκBα-KO mESCs (Figure 5).
380 This finding suggests that the observed role of IκBα in regulating the exit from naïve
381 pluripotency is not due to NF-κB inhibition. In fact, there is evidence that the chromatin
382 function of IκBα is an ancestral function preceding its role as NF-κB inhibitor. In
383 Caenorhabditis Elegans (*C.elegans*), which lacks NF-κB orthologs but possesses two homologs
384 of IκBα, the absence of IκBα orthologs has severe multi-organ differentiation defects (Brena
385 et al. 2020). This observation further supports the notion that the chromatin-related function

386 of IκBα plays a fundamental role in developmental processes, independent of its canonical
387 role in NF-κB signaling.

388 We have observed that IκBα-KO mESCs exhibit epigenetic and transcriptomic profiles
389 resembling the ground state of naïve pluripotency under Serum/LIF culture (Figure 3). In this
390 regard, the fact that IκBα is preferentially located in the chromatin of mESCs cultured in
391 Serum/LIF, when they exhibit a high degree of heterogeneity, suggests that IκBα might act as
392 a regulator of this heterogeneity. One potential explanation might be that IκBα could be
393 affecting the stability of fluctuating transcription factors, which is crucial to mediate the
394 pluripotent-to-differentiation balance (Martinez Arias and Brickman 2011). Thus, the lack of
395 IκBα might stabilize those transcription factors that would favor the ground-state observed in
396 IκBα-KO mESCs cultured in Serum/LIF. Further experiments are required to demonstrate this
397 hypothesis. Moreover, the differences in murine and human pluripotency (Weinberger et al.
398 2016) point out the necessity to address the real impact of IκBα modulation in the stabilization
399 of the ground state in human pluripotent stem cells. Our investigation has also revealed that
400 IκBα accumulates in the intergenic chromatin regions of naïve pluripotent cells (Figures 1D
401 and 4A). Mechanistically, this binding of IκBα serves to safeguard enhancers associated with
402 pluripotency from excessive activation. This is evidenced by the higher abundance of active
403 enhancers observed in IκBα-depleted mESCs, particularly in regions linked to pluripotency
404 located within TADs where IκBα is bound. A recent study highlights the significance of
405 maintaining a proper 3D chromatin architecture during the resolution of the naïve pluripotent
406 state (Lando et al. 2024). Our findings suggest that IκBα may potentially influence the 3D
407 conformation of regions relevant to pluripotency, thereby fine-tuning the expression of genes
408 crucial for sustaining naïve pluripotency (Figure 6). Nevertheless, the precise mechanisms by
409 which the absence of IκBα impacts 3D chromatin architecture remain to be elucidated.

410 In summary, our work establishes that IκBα mediates the exit from naïve pluripotency by
411 modulating the activation of enhancers associated with pluripotency genes. Importantly, this
412 newly identified role of IκBα operates independently of its canonical function in inhibiting the
413 NF-κB pathway. Our findings underscore the intricate interplay between inflammation and
414 pluripotency status, revealing a previously unrecognized complexity in their interaction.

415 **MATERIALS & METHODS**

416 **Cell culture**

417 mESC line ES-E14TG2a (ATCC; Cat #CRL-1821) was cultured on plastic dishes precoated with
418 0.1% (w/v) Gelatin (Sigma; Cat #G2500-100G) in Serum/LIF medium. Medium was changed
419 every day, and cells were passaged every other day using TrypLE Express (Gibco; Cat
420 #12605010) for harvesting. Cells were maintained in a 5% CO2 incubator at 37°C. For inducing
421 the ground-state of naïve pluripotency, mESCs were cultured in 2i/LIF medium for 2
422 consecutive passages.

423 **Epiblast stem cell differentiation**

424 Differentiation from mESCs towards Epiblast Stem Cells (EpiSCs) was performed as previously
425 described (Pantier et al. 2019). $3x10^4$ mESCs were seeded in 6-well plastic dishes, and they
426 were cultured in Serum/LIF medium for 24h. Medium was then switched to EpiSCs medium.
427 Cells were submitted to daily media changes till day 5 (120h), when they were further
428 analyzed.

429 **Embryoid bodies differentiation from mESCs**

430 Embryoid bodies (EBs) differentiation was established as described in (Sroczynska et al. 2009).
431 Briefly, mESCs were splitted twice in Serum/LIF medium before inducing differentiation. One
432 well of 6-well plate was splitted in an entire 6-well plate in IMDM-ES medium for 48h. mESCs
433 were then harvested, and they were rinsed twice with DPBS (Gibco; Cat #14190144). Cells
434 were very well disaggregated into single-cells, and 1.2 x 10^4 cells/mL embryoid body
435 differentiation (EB^{diff}) medium were resuspended to a total volume of 25mL of EB^{diff} medium.
436 EBs were formed in suspension for 5 days (120h). At day 5, in order to elongate the
437 differentiation up to 216h (day 9), EB^{diff} medium was refreshed by harvesting EBs with 10mL
438 serological pipette, centrifuge at 200 g for 3 min and EBs were resuspended in fresh EB^{diff}
439 medium for 4 more days.

440 Culture mediums composition are found in supplementary table 3.

441 **CRISPR/Cas9 gene editing and cell lines generation in mESCs**

442 The two guide RNAs (gRNAs) targeting the Nfkbia locus were designed using the CRISPR design
443 tool from MIT (http://crispr.mit.edu). The best 2 gRNAs (based on on-target and off-target
444 scores) that were targeting the exon 1 of Nfkbia (IκBα gene) were selected. After annealing,
445 one of the gRNAs was cloned into SpCas9(BB)-2A-GFP (px458) plasmid (Addgene; Cat #48138),
446 and the other gRNA was cloned into the px330-mCherry plasmid (modified from Addgene;
447 Cat #98750 to incorporate mCherry reporter). mESCs were co-transfected with the two
448 plasmids (px458-gRNA1 and px330-mCherry-gRNA2) by the use of Lipofectamine 200
449 following manufacturer's instructions (Invitrogen; Cat #11668019). GFP^+/$mCherry^+$ single cells

450 were FACS-purified. Mutant clones were screened through PCR and western blotting. Non-
451 targeting scrambled gRNAs were used as controls. Three independent clones from each
452 genotype (IκBα-WT and IκBα-KO) were selected for further experiments.

453 To increase IκBα specific detection, the IκBα endogenous gene (Nfkbia) was knocked-in with
454 3XFLAG sequence (DYKDHDGDYKDHDIDYKDDDDK) at the 3' end. To generate IκBα-3XFLAG
455 mESCs, 3XFLAG sequence was cloned into a plasmid containing Nfkbia left and right homology
456 arms flanking the endogenous stop codon; a spacer sequence of three glycines (GGCGGTGGG)
457 was also introduced. gRNAs and oligos sequences are included in supplementary table 1.

458 Doxycycline-inducible IκBα (IκBα^{WT}, IκBα$^{\Delta NF\text{-}\kappa B}$ and i-IκBα$^{\Delta H2A/H4}$) mESCs were generated by
459 cloning the three different IκBα versions into a PiggyBac transposon system (Chen et al. 2020).
460 IκBα protein-coding cDNAs were PCR-amplified, and the T2A-EGFP fragment was amplified
461 from PX458 and incorporated into the 3' end. PB-TRE was used as backbone (Addgene, Cat#
462 63800). Pool of transfected IκBα-KO mESCs was selected by Hygromycin (100µg/mL) for 7
463 days. Cells were doubly screened by FACS sorting green fluorescent protein after 24h of
464 doxycycline (1µg/mL) treatment. Pool of cells were used for further experiments. Oligos
465 sequences are included in supplementary table 1.

466 **Teratoma formation assay**

467 IκBα-WT and IκBα-KO mESCs grown in Serum/LIF (5×10^5) were injected intramuscularly into
468 severe combined immunodeficient mice (NSG). In order to favor 3D aggregation of cells and
469 teratoma formation, cells were resuspended in Matrigel Matrix (BD; Cat #356234) prior to
470 injection. Six weeks later, mice with tumors were euthanized, and tumors were fixed in
471 formaldehyde, embedded in paraffin, sectioned and stained with hematoxylin and eosin for
472 histological analysis.

473 **Immunofluorescence staining**

474 For immunostaining of mESCs, cells were seeded on 0.1% gelatin-coated coverslips on 6-well
475 plates; for EB immunofluorescence, they were collected directly from the plate. Samples were
476 washed twice with 1X PBS, and they were fixed at 4ºC for 30 minutes with 4% PFA (Electron
477 Microscopy Sciences; Cat #15713S). For immunofluorescence of 5-Methylcytosine (5mC),
478 fixed cells were incubated with 2M Hydrochloric Acid (Sigma-Aldrich, Cat #H1758) for 20
479 minutes at room temperature. Samples were then washed twice with 1X Tris-buffered saline
480 (TBS; 50 mM Tris-Cl, pH 8) and permeabilized and blocked with 1X TBS supplemented with 1%
481 Triton-X100 (MERCK; Cat #9036-19-5) and 6% FBS (Biological Industries; Cat #04-001-1A) for
482 2h at 4ºC. Samples were washed twice with 1X TBS supplemented with 6% FBS. Primary
483 antibody incubation was performed in 1X TBS plus 6% FBS and 0.3% or 0.5% Triton-X100 (0.3%
484 for 2D culture and 0.5% for EBs) overnight at 4ºC. Samples were then washed 4 times with 1X
485 TBS, 5 min each washing. Secondary antibody incubation was performed in TBS 1X plus 1%
486 BSA (Sigma-Aldrich; Cat #9048-46-8) for 2h at room temperature. Samples were washed three

487 times with 1X TBS for 5 min at room temperature each rinse. Samples were mounted using
488 DAPI Fluoromount-G (Southern Biotech; Cat #0100-20). List of antibodies used is found in
489 Supplementary table 2.

490 **Microscopy and image acquisition**

491 Fluorescence images were acquired using Confocal Leica TCS SP5 (Leica Microsystems), and
492 Leica application software LAS AF (Leica Microsystems) was used to visualize the images. The
493 Image J (version 1.15) was used for further analysis (Schneider et al. 2012).

494 **Flow cytometry sample preparation and analysis**

495 Cells were collected and purified based on FACS using BD FACSAria II Cell Sorter (BD
496 Bioscience). Cells were sorted at 3,500 events/second, and at maximum flow rate of 4 and 85
497 µm nozzle. 5 µg/ml of DAPI (Biotium; Cat #BT-40043) was used as a viability dye. For flow
498 cytometry analysis of pluripotency exit, cells were disaggregated using TrypLE Express, and
499 they were incubated at 4ºC for 20 minutes with the antibody. BD LSRFortessa Cell Analyzer or
500 BD LSR II Flow Cytometer (BD Bioscience) were used for Flow Cytometry Analysis experiments.
501 Flow cytometry data were analyzed using FlowJo X v10.0.7 (BD Biosciences).

502 **RNA isolation, cDNA synthesis and quantitative RT-PCR**

503 Total RNA isolation from cells was performed using the RNeasy Plus Mini Kit (Qiagen; Cat
504 #74136) or RNeasy Micro Kit (Qiagen; Cat #74004) following manufacturer's instructions.
505 Amount of RNA was quantified with Nanodrop (Thermo Fisher; Cat #ND2000CLAPTOP), and
506 2 µg of total RNA was retro-transcribed using Transcriptor First Strand cDNA Synthesis Kit
507 (Roche; Cat #04897030001) following the manufacturer's instructions.

508 Quantitative RT-PCR was performed in triplicates for each sample, and SYBR Green I Master
509 Kit (Roche; Cat #04887352001) was used to carry out the reaction. qRT-PCR was performed
510 using the LightCycler 480 system (Roche). Relative expression levels were calculated as $2^{-\Delta CT}$
511 normalized with the average CT of the housekeeping gene *Tbp* or *Gapdh*. Oligos sequences
512 are found in supplementary table 1.

513 **Chromatin Immunoprecipitation (ChIP)**

514 4-6x10^7 mESCs were cross-linked by incubating them in DPBS (Gibco, Cat #14190094)
515 supplemented with 1% formaldehyde (Sigma-Aldrich; Cat #252549) for 10 min rocking at
516 room temperature. Cross-linking was stopped using 125 mM Glycine (Sigma-Aldrich, Cat
517 #G8790) rocking for 5 minutes at room temperature. Fixed cells were then washed twice with
518 ice-cold DPBS, and scrapped and collected using DPBS supplemented with
519 protease/phosphatase inhibitor cocktail composed by 1X cOmplete™, EDTA-free Protease
520 Inhibitor Cocktail (Roche, Cat #11873580001), 1 mM PMSF, 1mM Sodium Ortovanadate and
521 20 mM β-Glycerol phosphate. Cells were centrifuged at 3200g for 5 minutes at 4ºC. Cells were

522 lysed by resuspending cell pellet in ice-cold ChIP buffer (1 volume of SDS buffer [100mM NaCl,
523 50mM Tris-HCl pH 8.1, 5mM EDTA pH 8, 0.5% SDS] and 0.5 volume of triton dilution buffer
524 [100mM Tris-HCl pH 8.6, 100mM NaCl, 5mM EDTA pH 8, 5% Triton X-100]) supplemented with
525 protease/phosphatase inhibitor cocktail, and samples were sonicated using sonication beads
526 (Diagenode; Cat #C01020031) and the Bioruptor Pico Sonicator (Diagenode; Cat #B01060010)
527 for 20 cycles (each cycle 30 seconds on/30 seconds off) or till DNA fragments have 100-300bp
528 size. Samples were centrifuged at 16000g for 20 minutes at 4ºC. Chromatin was quantified,
529 and 30 µg of chromatin was incubated with every 5µg of antibody rotating for 16 hours (or
530 overnight) at 4ºC. Samples were pulled down by incubation with Protein A-Sepharose™ CL-4B
531 (previously hydrated and blocked with 0.05% BSA) for 3h at 4ºC in rotation. Sample was
532 washed with a low salt washing buffer (50mM HEPES pH 7.5, 140mM NaCl and 1% Triton)
533 three times, one wash with a high salt wash buffer (50mM HEPES pH 7.5, 500mM NaCl and
534 1% Triton) and one wash with TE pH 8 (10mM Tris-HCl pH8, 1mM EDTA). Samples were then
535 eluted in 1% SDS and 100mM $NaHCO_3$. Samples were de-crosslinked by incubating for 16
536 hours (or overnight) at 65ºC shaking at 450 rpm, and were treated with Proteinase K for 1h at
537 45ºC. DNA was purified using QIAquick PCR Purification Kit (Qiagen, Cat #28106), following
538 the manufacturer's instructions.

539 For ChIP IκBα-3XFLAG, a previous cross-linking step using Gold (Diagenode, Cat #C01019027)
540 was performed following manufacturer's instructions, and cells (IκBα$^{3XFLAG/3XFLAG}$ and IκBα-WT
541 mESCs) were later treated with 1% formaldehyde as mentioned above. Cell nuclei were
542 isolated by incubating cell pellets in a buffer containing 5mM Pipes pH 8, 85mM KCl and 0.5%
543 NP40, and later incubated on ice for 10 minutes followed by centrifuge at 4000 rpm for 5
544 minutes at 4ºC. Nucleus were lysed in a buffer containing 1% SDS, 10mM EDTA and 50 mM
545 Tris-HCl pH 8.1 and incubated on ice for 10 min. Samples were sonicated as mentioned above
546 and SDS was removed by incubating the sonicated sample on ice for 1 hour and later
547 centrifuged for 15 at 4ºC and 16000g. 60µg of chromatin was incubated with 10 µg of
548 antibody. Samples were pulled down by a 50/50 mix of Dynabeads A (Invitrogen, Cat
549 #10002D) and G (Invitrogen, Cat #10003D). Samples were washed 4 times in 0.1% SDS, 1%
550 Triton-X, 2mM EDTA, 20mM Tris-HCl pH 8 and 150mM NaCl; followed by 1 wash in TE pH 8.
551 For ChIP followed by PCR, 1 µL of ChIP sample was normalized by its input. Oligos used are
552 found in supplementary table 1. For ChIP followed by sequencing (ChIP-seq) Purified DNA
553 concentration and integrity were determined using Agilent Bioanalyzer (Agilent Technologies;
554 Cat #G2939BA). Libraries were prepared using standard protocols. Chromatin was sequenced
555 using Illumina HiSeq platform (Illumina, Inc.) (50bp single-end reads). List of antibodies used
556 is found in Supplementary table 2.

557 **ChIP-seq data analysis**

558 Quality control was performed on raw data with FASTQC tool. Raw reads were trimmed to
559 remove adapters presence with Trimgalore (v0.6.6) (Ewels et al. 2012). Default parameters
560 were used except for a minimum quality of 15 (Phred score) and an adapter removal

561 stringency of 3bp overlap. For H3K4me3, H3K27me3, H3K4me1 and IκBα-3XFLAG or IκBα-
562 WT data, trimmed reads were aligned to reference genome with Bowtie2 (v2.4.4) which was
563 executed with default parameters (Langmead and Salzberg 2012). Required genome index
564 was built with corresponding GRCm38 fasta file retrieved from Ensembl
565 (http://ftp.ensembl.org/pub/release-102/). Multimapped reads and those exhibiting MAPQ <
566 20 were removed. For H3K9me3 data, trimmed reads were aligned to reference genome
567 (GRCm38 release 102 from Ensembl) with ShortStack (v3.8.5) (Axtell 2013). Randomly placed
568 multimappers were removed from the mapped reads. For all cases, duplicated reads were
569 marked with SAMtools (v1.15) (Danecek et al. 2021). Drosophila Melanogaster spike-ins,
570 present in H3K27me3, were discarded. NSC and RSC quality metrics were computed with
571 PhantomPeakQualTools (v1.2) (Landt et al. 2012). ENCODE blacklisted regions (mm10 v2)
572 were removed prior to peak calling except for H3K9me3 (Amemiya et al., 2019). BigWig files
573 were individually generated using deepTools (v3.5.1) bamCoverage with -ignoreDuplicates -
574 binSize 10 -smoothLength 30 -effectiveGenomeSize 2308125349 -normalizeUsing RPGC and -
575 extendReads *Fragment_Length* options (Ramírez et al. 2016). The effective genome size was
576 particularized to a read length of 50bp and directly retrieved from deepTools web site
577 (https://deeptools.readthedocs.io/en/develop/content/feature/effectiveGenomeSize.html).
578 *Fragment_Length* was retrieved from PhantomPeakQualTools results except for H3K9me3
579 where 150bp value was considered. Duplicates were kept in IκBα-3XFLAG for BigWig files
580 generation. For all histone marks except for H3K4me3, peak calling was conducted by means
581 of epic2 (v0.0.52) with -effective-genome-fraction 0.8452 -fragment-size *Fragment_Length*
582 options and chromosome sizes only referring to canonical chromosomes (Stovner and
583 Sætrom 2019). For H3K4me3 and IκBα-3XFLAG/WT, MACS2 (v2.2.7.1) was used to identify
584 peaks with -nomodel -extsize *Fragment_Length* -g 2308125349 options (Zhang et al. 2008).
585 The corresponding input sample was used in all peak calling computations. For the histone
586 marks, peaks were called with adjusted p-values (FDR) < 0.05. In case of IκBα-3XFLAG/WT
587 samples, peaks were called with adjusted p-values (FDR) < 0.05 and a minimum 4-fold
588 enrichment.

589 Peak annotation was performed with ChIPseeker R (v4.2.1) package (v1.34.1) considering a
590 TSS region range between 5000 bp upstream and 100 bp downstream (Yu et al., 2015).
591 Required TxDb object was generated from the Ensembl GRCm38 gtf file retrieved
592 (http://ftp.ensembl.org/pub/release-102/). A consensus peakset was obtained from the
593 three biological replicates per histone mark and condition (IκBα-WT or IκBα-KO) by identifying
594 overlapping peaks in at least two out of the three replicates. In case of IκBα ChIP-seq data,
595 peaks from consensus peakset identified from the -3XFLAG samples not overlapping with
596 IκBα-WT were considered the high-fidelity peaks for this experiment. For this purpose,
597 findOverlapsOfPeaks function from ChIPpeakAnno R package (v3.32.0) was used with default
598 parameters (Zhu et al. 2010).

599 Differential binding analysis (DBA) was conducted with DiffBind (v3.8.4) per histone mark
600 (Stark et al. 2011). Default parameters were used except for the summits parameter which

601 was set to 500bp for all histone marks except for H3K4me3 (150bp) in order to consider, for
602 testing, intervals of 1000bp or 300bp respectively. Summit values were selected to have
603 interval widths between the minimum and first quartile peak width values for each histone
604 mark. EdgeR was the statistical method used for all the three analyses. Differentially bound
605 regions (DBRs) between IκBα-KO and IκBα-WT samples were called with adjusted p-values
606 (FDR) < 0.05. Identified DBRs with any annotated gene were plotted with EnrichedHeatmap R
607 package (v1.18.1) (Gu et al. 2018). To summarize replicates per condition, normalizeToMatrix
608 function was used based on corresponding BigWig files in w0 mean mode in 50bp windows.
609 Tracks visualization were obtained by means of Integrative Genomics Browser (IGV) tool
610 (Robinson et al. 2011).

611 **Enhancers activity identification**

612 Consensus peaksets derived from the three H3K27ac and H3K4me1 IκBα-WT mESCs replicates
613 were used to identify poised and active enhancers in an IκBα-WT scenario. Putative poised
614 enhancers were defined as those regions with H3K4me1 but no H3K27ac peaks. Putative
615 active enhancers were defined as those regions with H3K27ac and presence/absence
616 H3K4me1 peaks. Putative gained or lost poised/active enhancers in IκBα-KO were obtained
617 with following criteria: (i) for gained/lost poised enhancers: a differential H3K4me1
618 increase/decrease and absence of H3K27ac peaks in IκBα-KO consensus peakset, (ii) for
619 gained/lost active enhancers (without H3K4me1): a differential H3K27ac increase/decrease
620 and absence of H3K4me1 in IκBα-KO consensus peakset and (iii) for gained/lost active
621 enhancers (with H3K4me1: a differential H3K27ac increase/decrease and presence of
622 H3K4me1 in IκBα-KO consensus peakset.

623 A maximum gap of 1000bp was allowed for checking the overlap between two different
624 histone marks. For this purpose, the 'subsetByOverlaps' function from the IRanges R package
625 was used (v.2.34.1).

626 **Hi-C data visualization and TADs annotations**

627 Juicebox v1.9.8 was run locally to visualize Hi-C data from (Bonev et al. 2017), specifically in
628 the mESCs (Serum/LIF) dataset. Corresponding maps from this dataset were already included
629 in the tool. To visualize contact maps, balanced normalization was considered and applied
630 color range up to 3 in the selected regions. Additionally, the list of 2,712 TADs with their
631 corresponding genome coordinates was retrieved and used to locate the IκBα peaks,
632 enhancers and showing differential activity together with differentially expressed genes from
633 in-house RNAseq data.

634 **RNA-seq experiments**

635 Total RNA from three independent clones from mESCs, 48h EBs and 96h EBs was isolated
636 using the RNeasy Plus Mini Kit (Qiagen; Cat #74136) following manufacturer's instructions.

637 RNA was quantified with Nanodrop (Thermo Fisher; Cat #ND2000CLAPTOP), and RNA
638 integrity was addressed by Agilent Bioanalyzer (Agilent Technologies; Cat #G2939BA).
639 Libraries sequenced using Illumina HiSeq 2500 (Illumina, Inc.) (125bp paired-end reads).
640 Samples sequencing depth ranged between 35M and 52M reads (average 41M reads) per
641 sample.

642 **RNA-seq data analysis**

643 Quality control was performed using FASTQC tool (v0.11.9). Raw reads were trimmed with
644 Trimgalore (v0.6.6) (Ewels et al. 2012). Default parameters were used except for a minimum
645 quality of 15 (Phred score) and an adapter removal stringency of 3bp overlap. Trimmed reads
646 were aligned to reference the genome with STAR aligner tool (v2.7.8). STAR was executed
647 with default parameters except for the number of allowed mismatches which was set to 1.
648 Genome index was built with corresponding GRCm38 gtf and fasta files retrieved from
649 Ensembl (http://ftp.ensembl.org/pub/release-102/). Obtained BAM files with uniquely
650 mapped reads were considered for further analysis. Raw gene expression was quantified
651 using featureCounts tool from subRead software (v2.0.1) with exon as feature (Liao et al.
652 2014). The raw counts matrix was imported into the R Statistical Software environment
653 (v4.2.1) for downstream analysis. Experimental design considered three timepoints: mouse
654 ESCs, EBs at 48h and EBs at 96h. Each time point included 6 samples distributed in two
655 conditions: 3 IκBα-WT and 3 IκBα-KO. Prior to statistical analysis, those genes with less than
656 10 raw counts across the 6 samples under test were removed. After pre-filtering, 21,843
657 genes (mESCs), 21,424 genes (EBs 48h) or 21,664 genes (EBs 96h) were available for testing.
658 For visualization purposes, counts were normalized by the variance-stabilizing transformation
659 method as implemented in DESeq2 R package (Love et al. 2014) (v1.38.3). Differential
660 expression analysis (DEA) was conducted with DESeq2. Each time point was independently
661 analyzed. Fitted statistical model included sample conditions as covariable with IκBα-WT as
662 the reference. Obtained $\log_2$ fold change values were shrunken with apeglm shrinkage
663 estimator R package (v1.20.0) (Zhu et al. 2019). Raw p-values were adjusted for multiple
664 testing using the Benjamini-Hochberg False Discovery Rate (FDR) (Benjamini and Hochberg
665 1995). Differentially Expressed Genes (DEGs) between IκBα-KO and IκBα-WT samples were
666 called with adjusted p-values (FDR) < 0.05 and absolute shrunken log2 Fold change > 1. Data
667 visualization was performed with the ggplot2 (v3.4.1).

668 **Genome-wide DNA methylation samples preparation**

669 DNA from frozen mESCs pellets was extracted using DNeasy Blood and Tissue Kit (Qiagen
670 GmbH, Hilden, Germany). Purified genomic DNA was quantified with Qubit (Invitrogen,
671 Carlsbad, CA, USA) according to manufacturer's instructions. Infinium Mouse Methylation
672 BeadChip (Illumina, Inc., San Diego, CA, USA) arrays were used to profile DNA methylation
673 genome wide. Samples were bisulfite converted using EZ DNA Methylation-Gold™ Kit (Zymo

674 Research, CA, USA) and were hybridized in the array following the manufacturer's
675 instructions.

676 **DNA methylation data analysis**

677 The DNA methylation profile of the studied samples was assessed using the Infinium Mouse
678 Methylation BeadChip Array (~285,000 methylation sites) as previously described (Garcia-
679 Prieto et al. 2022). Quality control steps to remove erratic probe signals were performed
680 within the R statistical environment (v4.0.3). We removed probes with detection p value >
681 0.01, genotyping probes and manufacturing flagged (MFG) probes described in the Illumina
682 manifest file (https://support.illumina.com/downloads/infinium-mouse-methylation-
683 manifest-file.html). The differentially methylated probes (DMPs) between IκBα-WT and IκBα-
684 KO samples were computed by deriving a linear model with the limma R package (v3.46.0).
685 Each condition included 3 samples per time point. DMPs with adjusted p-value (FDR) <0.05
686 and absolute mean methylation beta value difference between conditions >0.3 were
687 considered significant. DNA methylation analysis was performed using the mm10 mouse
688 genome reference build and the complete annotation was downloaded from the annotated
689 manifest file (http://zwdzwd.github.io/InfiniumAnnotation#mouse) (Zhou et al. 2022).

690 **Functional analysis**

691 Overrepresentation analysis was applied over lists of selected genes derived from RNA-seq
692 data (DEGs) or from ChIP-seq data (differentially bound regions). The Gene Ontology
693 (Biological Process ontology, GO BP terms), KEGG PATHWAY and WikiPathways databases for
694 Mus Musculus (Ashburner et al. 2000; Kanehisa and Goto 2000; Martens et al. 2021) were
695 interrogated by means of clusterProfiler R package (v4.6.2) (Wu et al., 2021). Corresponding
696 Entrez identifiers were used. Benjamini-Hochberg procedure was used to obtain adjusted p-
697 values. Obtained GO BP terms were simplified using the simplify function from clusterProfiler
698 with default parameters. Overrepresented terms or processes were called with adjusted p-
699 values (FDR) < 0.05.

700 Gene Set Enrichment Analysis (GSEA) was performed for mESCs against the three cell states
701 signatures defined by (Ghimire et al. 2018). Complete list of genes from mESCs samples
702 (21,843 genes) was ranked based on the shrunken log2 Fold Change obtained from DEA. GSEA
703 was conducted through the fgseaMultilevel function from fgsea R package (v1.24.0)
704 (Korotkevich et al. 2021) with default parameters. Enrichment plots were generated with the
705 same package.

706 Gene Set Variation Analysis (GSVA) R package (v1.46.0) with default parameters were used to
707 obtain Z-score values for genes annotated to endoderm (GO:0001706), mesoderm
708 (GO:0001707) and ectoderm (GO:0001705) GO BP terms (Hänzelmann et al. 2013).
709

Statistical analysis

Statistical analysis was performed with GraphPad Prism v.8.0.1. (GraphPad Software, Inc.). Unless specified, the comparison between two groups was performed with unpaired two-sided t-test. A p-value < 0.05 was considered significant.

DATA AVAILABILITY

Data is deposited at GEO under a SuperSeries with the accession number GSE239565)[https://www.ncbi.nlm.nih.gov/geo/query/acc.cgi?acc=GSE239565]. Individual SubSeries can be found at: GSE239563 (RNA-seq data), GSE239564 (ChIP-seq data) and GSE239562 (Methylation array data).

CODE AVAILABILITY

Scripts used to process the generated bulk RNA-seq and ChIP-seq data are available in Github repository: https://github.com/BigaSpinosaLab/IkBa_Naive_Pluripotency

COMPETING INTEREST STATEMENT

Authors declared no potential conflicts of interest.

ACKNOWLEDGEMENTS

We would like to acknowledge all members of the Bigas/Espinosa labs for helpful discussions. We are grateful for technical support to CRG/UPF Flow Cytometry Unit, CRG Genomics and Advanced Light Microscopy Units. This work has been supported by Spanish Ministry of Science and Innovation (PID2019-104695RB-I00, PLEC2021-007518, PDC2021-120817-I00), Generalitat de Catalunya (2021SGR/39) and Departament de Salut (SLT002/16/00299) to AB; the Spanish Ministry of Science and Innovation (PID2019-108322GB-100 and PID2022-142679NB-I00) to LDC; the Spanish Ministry of Science and Innovation (PID2021-123383NB-I00.) and the Agencia de Gestió d'Ajuts Universitaris i de Recerca (2021 SGR 01222) to BP. L.G.P has been a recipient of FI AGAUR fellowship (2019 FI-B 00151/2020 FI_B1 00130) from Generalitat de Catalunya. D.A-V was funded by the FIS fellowship (FI20/00130) from Instituto Carlos III. M.B. received funding from the Ramón Areces Foundation. M.M. is a recipient of a grant from the Instituto Carlos III, grant number CA22/00011 (co-funded by the European Social Fund Plus, ESF+ and by the European Union).

Author contributions

L.G.P, L.E and A.B designed the study. L.G.P, D.A-V, M.B, A.I, J.G, J.B, D.A.E, C.A.G.P, C.B, V.R.C and A.V performed experiments. L.G.P, M.M, M.B and C.A.G.P performed bioinformatics analysis. L.G and A.B wrote the manuscript with input from all authors. C.B, A.V, A.V, P.M,

L.D.C, G.S, B.P, M.E and L.E provided input on experimental design. L.E and A.B provided resources and supervised the research.

745 **REFERENCES**

746 Aguilera C, Hoya-Arias R, Haegeman G, Espinosa L, Bigas A. 2004. Recruitment of IκBα
747 to the *hes1* promoter is associated with transcriptional repression. *Proceedings of the*
748 *National Academy of Sciences* **101**: 16537–16542.

749 Alvarez-Villanueva D, Galan L, Bertran J, Floor M. 2023. Separation-of-function mutants
750 reveal the NF-κB-independent involvement of IκBα in the regulation of stem cell and
751 oncogenic programs. *bioRxiv*.
752 https://www.biorxiv.org/content/10.1101/2023.06.21.545928.abstract.

753 Álvarez-Villanueva D, Galán-Palma L, Bertran J, Floor M, Solé L, Lobo-Jarne T, Maqueda
754 M, Rajbhandari R, Marruecos L, Villà-Freixa J, et al. 2023. Separation-of-function
755 mutants reveal the NF-κB-independent involvement of IκBα in the regulation of stem
756 cell and oncogenic programs. *bioRxiv* 2023.06.21.545928.
757 https://www.biorxiv.org/content/10.1101/2023.06.21.545928v1 (Accessed July 17,
758 2023).

759 Ashburner M, Ball CA, Blake JA, Botstein D, Butler H, Cherry JM, Davis AP, Dolinski K,
760 Dwight SS, Eppig JT, et al. 2000. Gene ontology: tool for the unification of biology. The
761 Gene Ontology Consortium. *Nat Genet* **25**: 25–29.

762 Atlasi Y, Jafarnejad SM, Gkogkas CG, Vermeulen M, Sonenberg N, Stunnenberg HG.
763 2020. The translational landscape of ground state pluripotency. *Nat Commun* **11**: 1617.

764 Axtell MJ. 2013. ShortStack: comprehensive annotation and quantification of small RNA
765 genes. *RNA* **19**: 740–751.

766 Bao S, Tang F, Li X, Hayashi K, Gillich A, Lao K, Surani MA. 2009. Epigenetic reversion of
767 post-implantation epiblast to pluripotent embryonic stem cells. *Nature* **461**: 1292–
768 1295.

769 Basak S, Kim H, Kearns JD, Tergaonkar V, O'Dea E, Werner SL, Benedict CA, Ware CF,
770 Ghosh G, Verma IM, et al. 2007. A fourth IkappaB protein within the NF-kappaB
771 signaling module. *Cell* **128**: 369–381.

772 Benjamini Y, Hochberg Y. 1995. Controlling the False Discovery Rate: A Practical and
773 Powerful Approach to Multiple Testing. *J R Stat Soc Series B Stat Methodol* **57**: 289–
774 300.

775 Bleckwehl T, Crispatzu G, Schaaf K, Respuela P, Bartusel M, Benson L, Clark SJ, Dorighi
776 KM, Barral A, Laugsch M, et al. 2021. Enhancer-associated H3K4 methylation
777 safeguards in vitro germline competence. *Nat Commun* **12**: 5771.

778 Bonev B, Mendelson Cohen N, Szabo Q, Fritsch L, Papadopoulos GL, Lubling Y, Xu X, Lv
779 X, Hugnot J-P, Tanay A, et al. 2017. Multiscale 3D Genome Rewiring during Mouse
780 Neural Development. *Cell* **171**: 557–572.e24.

781 Boroviak T, Loos R, Lombard P, Okahara J, Behr R, Sasaki E, Nichols J, Smith A, Bertone

782 P. 2015. Lineage-Specific Profiling Delineates the Emergence and Progression of Naive
783 Pluripotency in Mammalian Embryogenesis. *Dev Cell* **35**: 366–382.

784 Brena D, Bertran J, Porta-de-la-Riva M, Guillén Y, Cornes E, Kukhtar D, Campos-Vicens L,
785 Fernández L, Pecharroman I, García-López A, et al. 2020. Ancestral function of
786 Inhibitors-of-kappaB regulates Caenorhabditis elegans development. *Sci Rep* **10**: 16153.

787 Brons IGM, Smithers LE, Trotter MWB, Rugg-Gunn P, Sun B, Chuva de Sousa Lopes SM,
788 Howlett SK, Clarkson A, Ahrlund-Richter L, Pedersen RA, et al. 2007. Derivation of
789 pluripotent epiblast stem cells from mammalian embryos. *Nature* **448**: 191–195.

790 Buecker C, Srinivasan R, Wu Z, Calo E, Acampora D, Faial T, Simeone A, Tan M, Swigut T,
791 Wysocka J. 2014. Reorganization of enhancer patterns in transition from naive to
792 primed pluripotency. *Cell Stem Cell* **14**: 838–853.

793 Chen Q, Luo W, Veach RA, Hickman AB, Wilson MH, Dyda F. 2020. Structural basis of
794 seamless excision and specific targeting by piggyBac transposase. *Nat Commun* **11**:
795 3446.

796 Choi J, Huebner AJ, Clement K, Walsh RM, Savol A, Lin K, Gu H, Di Stefano B,
797 Brumbaugh J, Kim S-Y, et al. 2017. Prolonged Mek1/2 suppression impairs the
798 developmental potential of embryonic stem cells. *Nature* **548**: 219–223.

799 Danecek P, Bonfield JK, Liddle J, Marshall J, Ohan V, Pollard MO, Whitwham A, Keane T,
800 McCarthy SA, Davies RM, et al. 2021. Twelve years of SAMtools and BCFtools.
801 *Gigascience* **10**. http://dx.doi.org/10.1093/gigascience/giab008.

802 Di Stefano B, Luo E-C, Haggerty C, Aigner S, Charlton J, Brumbaugh J, Ji F, Rabano
803 Jiménez I, Clowers KJ, Huebner AJ, et al. 2019. The RNA Helicase DDX6 Controls Cellular
804 Plasticity by Modulating P-Body Homeostasis. *Cell Stem Cell* **25**: 622–638.e13.

805 Dutta D, Ray S, Home P, Larson M, Wolfe MW, Paul S. 2011. Self-renewal versus lineage
806 commitment of embryonic stem cells: protein kinase C signaling shifts the balance.
807 *Stem Cells* **29**: 618–628.

808 Espín-Palazón R, Traver D. 2016. The NF-κB family: Key players during embryonic
809 development and HSC emergence. *Exp Hematol* **44**: 519–527.

810 Ewels P, Afyounian E, Schuster-Boeckler BFK. 2012. TrimGalore: v0. 6.7-DOI via
811 Zenodo.(Zenodo, 2021). doi: 10.5281/zenodo. 5127899. 2. Langmead, B. & Salzberg, SL
812 Fast gapped-read alignment with …. *Nat Methods*.

813 Factor DC, Corradin O, Zentner GE, Saiakhova A, Song L, Chenoweth JG, McKay RD,
814 Crawford GE, Scacheri PC, Tesar PJ. 2014. Epigenomic comparison reveals activation of
815 "seed" enhancers during transition from naive to primed pluripotency. *Cell Stem Cell*
816 **14**: 854–863.

817 Festuccia N, Osorno R, Wilson V, Chambers I. 2013. The role of pluripotency gene
818 regulatory network components in mediating transitions between pluripotent cell

819 states. *Curr Opin Genet Dev* **23**: 504–511.

820 Garcia-Prieto CA, Álvarez-Errico D, Musulen E, Bueno-Costa A, N. Vazquez B, Vaquero
821 A, Esteller M. 2022. Validation of a DNA methylation microarray for 285,000 CpG sites
822 in the mouse genome. *Epigenetics* **17**: 1677–1685.

823 Gerondakis S, Grumont R, Gugasyan R, Wong L, Isomura I, Ho W, Banerjee A. 2006.
824 Unravelling the complexities of the NF-kappaB signalling pathway using mouse
825 knockout and transgenic models. *Oncogene* **25**: 6781–6799.

826 Ghimire S, Van der Jeught M, Neupane J, Roost MS, Anckaert J, Popovic M, Van
827 Nieuwerburgh F, Mestdagh P, Vandesompele J, Deforce D, et al. 2018. Comparative
828 analysis of naive, primed and ground state pluripotency in mouse embryonic stem cells
829 originating from the same genetic background. *Sci Rep* **8**: 5884.

830 Graf T, Stadtfeld M. 2008. Heterogeneity of embryonic and adult stem cells. *Cell Stem*
831 *Cell* **3**: 480–483.

832 Guo G, Yang J, Nichols J, Hall JS, Eyres I, Mansfield W, Smith A. 2009. Klf4 reverts
833 developmentally programmed restriction of ground state pluripotency. *Development*
834 **136**: 1063–1069.

835 Guo Y-L. 2019. The underdeveloped innate immunity in embryonic stem cells: The
836 molecular basis and biological perspectives from early embryogenesis. *Am J Reprod*
837 *Immunol* **81**: e13089.

838 Gu Z, Eils R, Schlesner M, Ishaque N. 2018. EnrichedHeatmap: an R/Bioconductor
839 package for comprehensive visualization of genomic signal associations. *BMC Genomics*
840 **19**: 234.

841 Habibi E, Brinkman AB, Arand J, Kroeze LI, Kerstens HHD, Matarese F, Lepikhov K, Gut
842 M, Brun-Heath I, Hubner NC, et al. 2013. Whole-genome bisulfite sequencing of two
843 distinct interconvertible DNA methylomes of mouse embryonic stem cells. *Cell Stem*
844 *Cell* **13**: 360–369.

845 Hänzelmann S, Castelo R, Guinney J. 2013. GSVA: gene set variation analysis for
846 microarray and RNA-seq data. *BMC Bioinformatics* **14**: 7.

847 Hayden MS, Ghosh S. 2008. Shared principles in NF-kappaB signaling. *Cell* **132**: 344–
848 362.

849 Hu S, Metcalf E, Mahat DB, Chan L, Sohal N, Chakraborty M, Hamilton M, Singh A, Singh
850 A, Lees JA, et al. 2022. Transcription factor antagonism regulates heterogeneity in
851 embryonic stem cell states. *Mol Cell* **82**: 4410–4427.e12.

852 Kaltschmidt C, Greiner JFW, Kaltschmidt B. 2021. The Transcription Factor NF-κB in
853 Stem Cells and Development. *Cells* **10**. http://dx.doi.org/10.3390/cells10082042.

854 Kanehisa M, Goto S. 2000. KEGG: kyoto encyclopedia of genes and genomes. *Nucleic*

855 *Acids Res* **28**: 27–30.

856 Korotkevich G, Sukhov V, Budin N, Shpak B, Artyomov MN, Sergushichev A. 2021. Fast
857 gene set enrichment analysis. *bioRxiv* 060012.
858 https://www.biorxiv.org/content/10.1101/060012v3 (Accessed March 11, 2024).

859 Lando D, Ma X, Cao Y, Jartseva A, Stevens TJ, Boucher W, Reynolds N, Montibus B, Hall
860 D, Lackner A, et al. 2024. Enhancer-promoter interactions are reconfigured through the
861 formation of long-range multiway hubs as mouse ES cells exit pluripotency. *Mol Cell* **84**:
862 1406–1421.e8.

863 Landt SG, Marinov GK, Kundaje A, Kheradpour P, Pauli F, Batzoglou S, Bernstein BE,
864 Bickel P, Brown JB, Cayting P, et al. 2012. ChIP-seq guidelines and practices of the
865 ENCODE and modENCODE consortia. *Genome Res* **22**: 1813–1831.

866 Langmead B, Salzberg SL. 2012. Fast gapped-read alignment with Bowtie 2. *Nat*
867 *Methods* **9**: 357–359.

868 Leitch HG, McEwen KR, Turp A, Encheva V, Carroll T, Grabole N, Mansfield W, Nashun
869 B, Knezovich JG, Smith A, et al. 2013. Naive pluripotency is associated with global DNA
870 hypomethylation. *Nat Struct Mol Biol* **20**: 311–316.

871 Liao Y, Smyth GK, Shi W. 2014. featureCounts: an efficient general purpose program for
872 assigning sequence reads to genomic features. *Bioinformatics* **30**: 923–930.

873 Lieberman-Aiden E, van Berkum NL, Williams L, Imakaev M, Ragoczy T, Telling A, Amit I,
874 Lajoie BR, Sabo PJ, Dorschner MO, et al. 2009. Comprehensive mapping of long-range
875 interactions reveals folding principles of the human genome. *Science* **326**: 289–293.

876 Li S, Sun J, Zhang B-W, Yang L, Wan Y-C, Chen B-B, Xu N, Xu Q-R, Fan J, Shang J-N, et al.
877 2024. ATG5 attenuates inflammatory signaling in mouse embryonic stem cells to
878 control differentiation. *Dev Cell*. http://dx.doi.org/10.1016/j.devcel.2024.01.026.

879 Love MI, Huber W, Anders S. 2014. Moderated estimation of fold change and
880 dispersion for RNA-seq data with DESeq2. *Genome Biol* **15**: 550.

881 Marks H, Kalkan T, Menafra R, Denissov S, Jones K, Hofemeister H, Nichols J, Kranz A,
882 Stewart AF, Smith A, et al. 2012. The transcriptional and epigenomic foundations of
883 ground state pluripotency. *Cell* **149**: 590–604.

884 Marruecos L, Bertran J, Álvarez-Villanueva D, Mulero MC, Guillén Y, Palma LG, Floor M,
885 Vert A, Arce-Gallego S, Pecharroman I, et al. 2021. Dynamic chromatin association of
886 IκBα is regulated by acetylation and cleavage of histone H4. *EMBO Rep* **22**: e52649.

887 Marruecos L, Bertran J, Guillén Y, González J, Batlle R, López-Arribillaga E, Garrido M,
888 Ruiz-Herguido C, Lisiero D, González-Farré M, et al. 2020. IκBα deficiency imposes a
889 fetal phenotype to intestinal stem cells. *EMBO Rep* **21**: e49708.

890 Martens M, Ammar A, Riutta A, Waagmeester A, Slenter DN, Hanspers K, A Miller R,

891 Digles D, Lopes EN, Ehrhart F, et al. 2021. WikiPathways: connecting communities.
892 *Nucleic Acids Res* **49**: D613–D621.

893 Martinez Arias A, Brickman JM. 2011. Gene expression heterogeneities in embryonic
894 stem cell populations: origin and function. *Curr Opin Cell Biol* **23**: 650–656.

895 Mulero MC, Ferres-Marco D, Islam A, Margalef P, Pecoraro M, Toll A, Drechsel N,
896 Charneco C, Davis S, Bellora N, et al. 2013. Chromatin-bound IκBα regulates a subset of
897 polycomb target genes in differentiation and cancer. *Cancer Cell* **24**: 151–166.

898 Pantier R, Tatar T, Colby D, Chambers I. 2019. Endogenous epitope-tagging of Tet1,
899 Tet2 and Tet3 identifies TET2 as a naïve pluripotency marker. *Life Sci Alliance* **2**.
900 http://dx.doi.org/10.26508/lsa.201900516.

901 Pera MF, Rossant J. 2021. The exploration of pluripotency space: Charting cell state
902 transitions in peri-implantation development. *Cell Stem Cell* **28**: 1896–1906.

903 Ramírez F, Ryan DP, Grüning B, Bhardwaj V, Kilpert F, Richter AS, Heyne S, Dündar F,
904 Manke T. 2016. deepTools2: a next generation web server for deep-sequencing data
905 analysis. *Nucleic Acids Res* **44**: W160–5.

906 Robinson JT, Thorvaldsdóttir H, Winckler W, Guttman M, Lander ES, Getz G, Mesirov JP.
907 2011. Integrative genomics viewer. *Nat Biotechnol* **29**: 24–26.

908 Schneider CA, Rasband WS, Eliceiri KW. 2012. NIH Image to ImageJ: 25 years of image
909 analysis. *Nat Methods* **9**: 671–675.

910 Singer ZS, Yong J, Tischler J, Hackett JA, Altinok A, Surani MA, Cai L, Elowitz MB. 2014.
911 Dynamic heterogeneity and DNA methylation in embryonic stem cells. *Mol Cell* **55**:
912 319–331.

913 Sroczynska P, Lancrin C, Pearson S, Kouskoff V, Lacaud G. 2009. In vitro differentiation
914 of mouse embryonic stem cells as a model of early hematopoietic development.
915 *Methods Mol Biol* **538**: 317–334.

916 Stark R, Brown G, Others. 2011. DiffBind: differential binding analysis of ChIP-Seq peak
917 data. *R package version* **100**.
918 https://www.andersvercelli.com/packages/2.13/bioc/vignettes/DiffBind/inst/doc/DiffB
919 ind.pdf.

920 Stovner EB, Sætrom P. 2019. epic2 efficiently finds diffuse domains in ChIP-seq data.
921 *Bioinformatics* **35**: 4392–4393.

922 Takahashi S, Kobayashi S, Hiratani I. 2018. Epigenetic differences between naïve and
923 primed pluripotent stem cells. *Cell Mol Life Sci* **75**: 1191–1203.

924 Tesar PJ, Chenoweth JG, Brook FA, Davies TJ, Evans EP, Mack DL, Gardner RL, McKay
925 RDG. 2007. New cell lines from mouse epiblast share defining features with human
926 embryonic stem cells. *Nature* **448**: 196–199.

927 Thambyrajah R, Fadlullah Z, Proffitt M, Neo WH, Guillén Y, Casado-Pelaez M, Herrero-
928 Molinero P, Brujas C, Castelluccio N, González J, et al. 2022. IκBα controls dormancy
929 induction in Hematopoietic stem cell development via retinoic acid. *bioRxiv*
930 2022.11.17.516971. https://www.biorxiv.org/content/10.1101/2022.11.17.516971v1
931 (Accessed July 11, 2023).

932 Torres J, Watt FM. 2008. Nanog maintains pluripotency of mouse embryonic stem cells
933 by inhibiting NFkappaB and cooperating with Stat3. *Nat Cell Biol* **10**: 194–201.

934 Wang X, Wu Q. 2022. The Divergent Pluripotent States in Mouse and Human Cells.
935 *Genes* **13**. http://dx.doi.org/10.3390/genes13081459.

936 Weinberger L, Ayyash M, Novershtern N, Hanna JH. 2016. Dynamic stem cell states:
937 naive to primed pluripotency in rodents and humans. *Nat Rev Mol Cell Biol* **17**: 155–
938 169.

939 Wu X, Wu X, Xie W. 2023. Activation, decommissioning, and dememorization:
940 enhancers in a life cycle. *Trends Biochem Sci* **48**: 673–688.

941 Yagi M, Kishigami S, Tanaka A, Semi K, Mizutani E, Wakayama S, Wakayama T,
942 Yamamoto T, Yamada Y. 2017. Derivation of ground-state female ES cells maintaining
943 gamete-derived DNA methylation. *Nature* **548**: 224–227.

944 Ying Q-L, Wray J, Nichols J, Batlle-Morera L, Doble B, Woodgett J, Cohen P, Smith A.
945 2008. The ground state of embryonic stem cell self-renewal. *Nature* **453**: 519–523.

946 Zhang Q, Lenardo MJ, Baltimore D. 2017. 30 Years of NF-κB: A Blossoming of Relevance
947 to Human Pathobiology. *Cell* **168**: 37–57.

948 Zhang Y, Liu T, Meyer CA, Eeckhoute J, Johnson DS, Bernstein BE, Nusbaum C, Myers
949 RM, Brown M, Li W, et al. 2008. Model-based analysis of ChIP-Seq (MACS). *Genome*
950 *Biol* **9**: R137.

951 Zhou W, Hinoue T, Barnes B, Mitchell O, Iqbal W, Lee SM, Foy KK, Lee K-H, Moyer EJ,
952 VanderArk A, et al. 2022. DNA methylation dynamics and dysregulation delineated by
953 high-throughput profiling in the mouse. *Cell Genom* **2**.
954 http://dx.doi.org/10.1016/j.xgen.2022.100144.

955 Zhou W, Triche TJ Jr, Laird PW, Shen H. 2018. SeSAMe: reducing artifactual detection of
956 DNA methylation by Infinium BeadChips in genomic deletions. *Nucleic Acids Res* **46**:
957 e123.

958 Zhu A, Ibrahim JG, Love MI. 2019. Heavy-tailed prior distributions for sequence count
959 data: removing the noise and preserving large differences. *Bioinformatics* **35**: 2084–
960 2092.

961 Zhu LJ, Gazin C, Lawson ND, Pagès H, Lin SM, Lapointe DS, Green MR. 2010.
962 ChIPpeakAnno: a Bioconductor package to annotate ChIP-seq and ChIP-chip data. *BMC*
963 *Bioinformatics* **11**: 237.

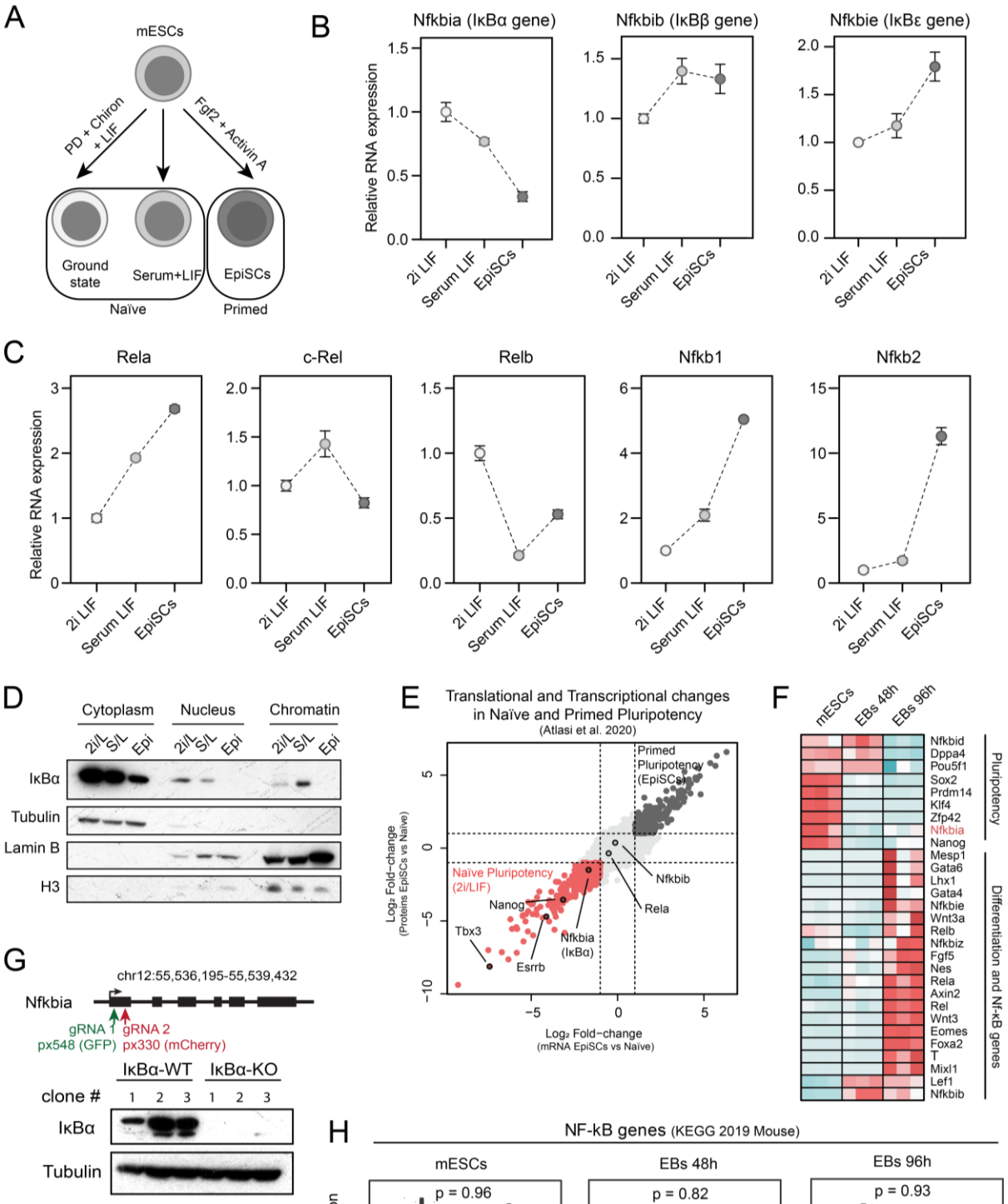
A
mESCs
PD + Chiron + LIF
Fgf2 + Activin A
Ground state
Serum+LIF
EpiSCs
Naïve
Primed
B
Nfkbia (IκBα gene)
Nfkbib (IκBβ gene)
Nfkbie (IκBε gene)
Relative RNA expression
2i LIF
Serum LIF
EpiSCs
C
Rela
c-Rel
Relb
Nfkb1
Nfkb2
D
Cytoplasm
Nucleus
Chromatin
2i/L
S/L
Epi
IκBα
Tubulin
Lamin B
H3
E
Translational and Transcriptional changes in Naïve and Primed Pluripotency
(Atlasi et al. 2020)
Primed Pluripotency (EpiSCs)
Naïve Pluripotency (2i/LIF)
Nfkbib
Rela
Nanog
Tbx3
Nfkbia (IκBα)
Esrrb
Log₂ Fold-change (Proteins EpiSCs vs Naïve)
Log₂ Fold-change (mRNA EpiSCs vs Naïve)
F
mESCs
EBs 48h
EBs 96h
Nfkbid
Dppa4
Pou5f1
Sox2
Prdm14
Klf4
Zfp42
Nfkbia
Nanog
Mesp1
Gata6
Lhx1
Gata4
Nfkbie
Wnt3a
Relb
Nfkbiz
Fgf5
Nes
Rela
Axin2
Rel
Wnt3
Eomes
Foxa2
T
Mixl1
Lef1
Nfkbib
Pluripotency
Differentiation and NF-κB genes
G
chr12:55,536,195-55,539,432
Nfkbia
gRNA 1
px548 (GFP)
gRNA 2
px330 (mCherry)
IκBα-WT
IκBα-KO
clone #
1 2 3 1 2 3
IκBα
Tubulin
H
NF-κB genes (KEGG 2019 Mouse)
mESCs
EBs 48h
EBs 96h
p = 0.96
p = 0.82
p = 0.93
Normalized Expression
IκBα-WT
IκBα-KO

964

965

966 **Figure 1. IκBα specifically accumulates in the chromatin of the naïve pluripotent state. A.**
967 Schematic of pluripotent states in mouse embryonic stem cells (mESCs). **B. C.** Relative mRNA
968 levels of the canonical IκB genes (**B**) or Nf-κB effector genes (**C**). Expression was normalized
969 using the house-keeping gene *Tbp* relative to 2i/LIF. Data from three independent
970 experiments. Dots indicate mean values and error bars refer to ± standard deviation (SD). **D.**
971 Western blot analysis of IκBα protein distribution in cytoplasm, nucleoplasm (Nucleus) or
972 chromatin in cells at different pluripotency states. **E.** Transcriptome and proteome differences
973 between 2i/LIF and EpiSCs. Enriched transcripts and proteins in naïve or primed states are
974 highlighted in red or dark gray, respectively (Log_2 fold-change < -1 or >1, respectively). Data
975 from (Atlasi et al. 2020). **F.** Heatmap showing the expression levels of pluripotency (*Dppa4,*
976 *Pou5f1, Sox2, Prdm14, Klf4, Zfp42, Nanog*), differentiation (*Mesp1, Gata4, Gata6, Lhx1,*
977 *Wnt3a, Fgf5, Nes, Axin2, Wnt3, Eomes, Foxa2, T, Mixl1, Lef1*) and NF-κB (*Nfkbia, Nfkbib,*
978 *Nfkbie, Nfkbiz, Rela, c-Rel, Relb*) genes from the RNAseq samples in mESCs and differentiating
979 cells (embryoid bodies) at 48h and 96h of IκBα-WT cells. **G.** Schematic to deplete IκBα protein
980 in mESCs (upper panel) and western blot analysis of three independent IκBα-WT and IκBα-KO
981 mESC clones (bottom panel). **H.** Boxplots, violin plots and individual values representing the
982 normalized gene expression levels in IκBα-WT or IκBα-KO mESCs, EBs 48h and EBs 96h.
983 Considered genes are those annotated to NF-κB signaling pathway (KEGG). Unpaired two-
984 sided Wilcoxon test applied.

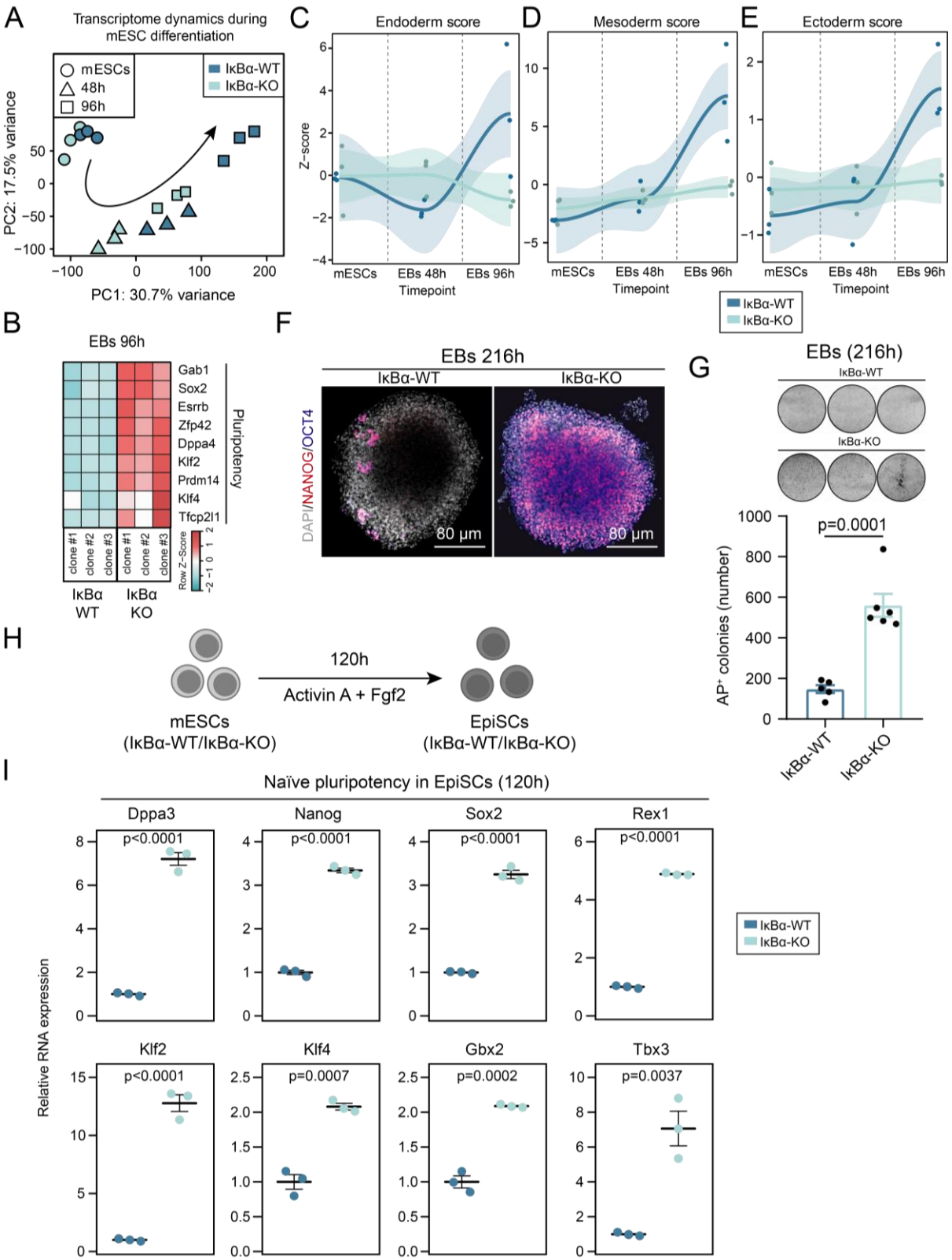

985

986

987 **Figure 2. Lack of IκBα impairs the exit from naïve pluripotency. A.** PC1 and PC2 from Principal
988 Component Analysis (PCA) of normalized RNA-seq data from mESCs, 48h EBs and 96h EBs of
989 IκBα-WT and IκBα-KO cells (three independent clones from each genotype). **B.** Expression

level of naïve pluripotency genes in IκBα-WT and IκBα-KO 96h EBs. **C, D, E**. Expression of endoderm (C), mesoderm (D) and ectoderm (E) genes from Gene Ontology (GO) database at mESCs, 48h and 96h EBs IκBα-WT or IκBα-KO cells (three independent clones). Loess curves are also represented with 95% confidence intervals. **F.** Representative immunofluorescence of 216h EBs stained with NANOG and OCT3/4. **G.** Quantification of total number of alkaline phosphatase (AP) colonies after 216h EB differentiation and additional culture of 96h in Serum/LIF (S/L) medium. Dots represent values from two independent experiments from three different IκBα-WT or IκBα-KO clones. Unpaired two-sided t-test applied. **H.** Schematics of mESCs differentiation to EpiSCs (Materials and Methods section for further information). **I.** Relative RNA levels of naïve pluripotency genes in IκBα-WT or IκBα-KO EpiSCs at 120h. RNA levels were normalized based on *Tbp* expression relative to IκBα-WT. Each dot represents an independent clone. Unpaired two-sided t-test applied. Error bars refer to ± SD.

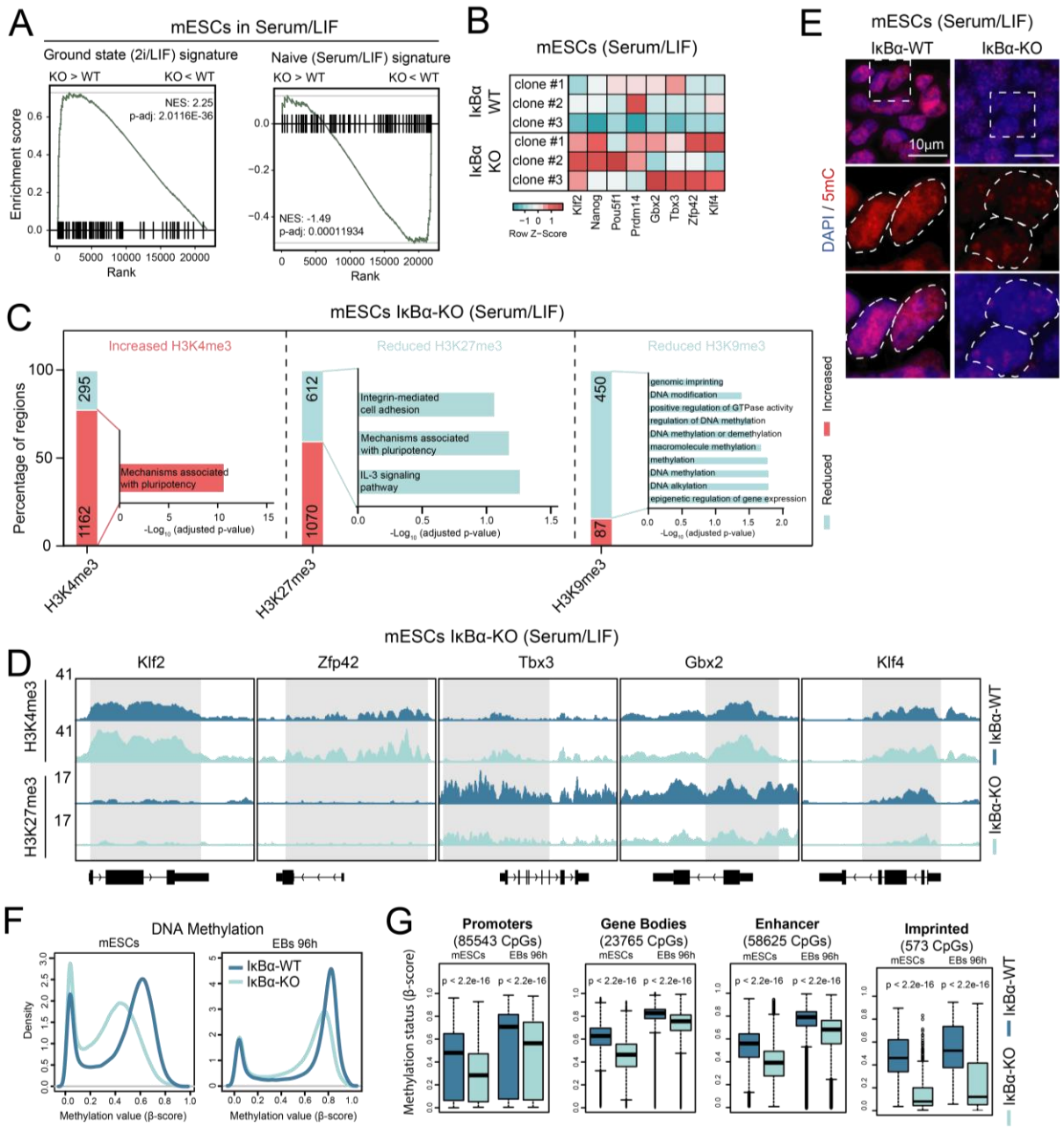

Figure 3. IκBα-KO mESCs preserve the ground-state of naïve pluripotency under Serum/LIF culture. A. GSEA results comparing IκBα-KO vs IκBα-WT mESCs cultured in Serum/LIF against ground (2i/LIF) and naïve (Serum/LIF) state pluripotency signatures from (Ghimire et al. 2018). Adjusted p-value by Benjamini-Hochberg procedure and Normalized Enrichment Score (NES) indicated. **B.** Expression of the naïve pluripotency genes from the RNAseq samples of IκBα-KO and IκBα-WT mESCs cultured in Serum/LIF. **C.** Number of differentially bound regions (adjusted p-value <0.05, FDR) for H3K4me3, H3K27me3 and H3K9me3 in IκBα$^{-/-}$ vs IκBα$^{+/+}$ mESCs cultured in Serum/LIF. Enriched or reduced regions in IκBα $^{-/-}$ mESCs are distinguished ($\log_2$ Fold-change >0 or <0, respectively). Overrepresented WikiPathways for (left) H3K4me3 and (center) H3K27me3, or GO terms for (right) H3K9me3 (adjusted p-value < 0.05, FDR) are indicated. A one-sided hypergeometric test was conducted. **D.** Representative naïve pluripotency genes having differential H3K4me3 (enriched) and H3K27me3 (reduced) levels

1016 in IκBα $^{-/-}$ vs IκBα $^{+/+}$ mESCs cultured in Serum/LIF. Shadowed regions highlight the differential
1017 levels of the histone marks. **E.** Representative immunofluorescence images of DNA-
1018 methylation-related mark 5-methylcytosine (5mC) in IκBα-WT (left) and IκBα-KO (right)
1019 mESCs cultured in Serum/LIF. **F.** DNA methylation profile in IκBα-WT vs IκBα-KO mESCs (left)
1020 and 96h EBs (right) showing the distribution density of mean ß-values from all 261,220 CpGs.
1021 **G.** DNA methylation levels in different genomic regions in either IκBα-WT vs IκBα-KO mESCs
1022 or 96h EBs. Unpaired two-sided t-test was applied.

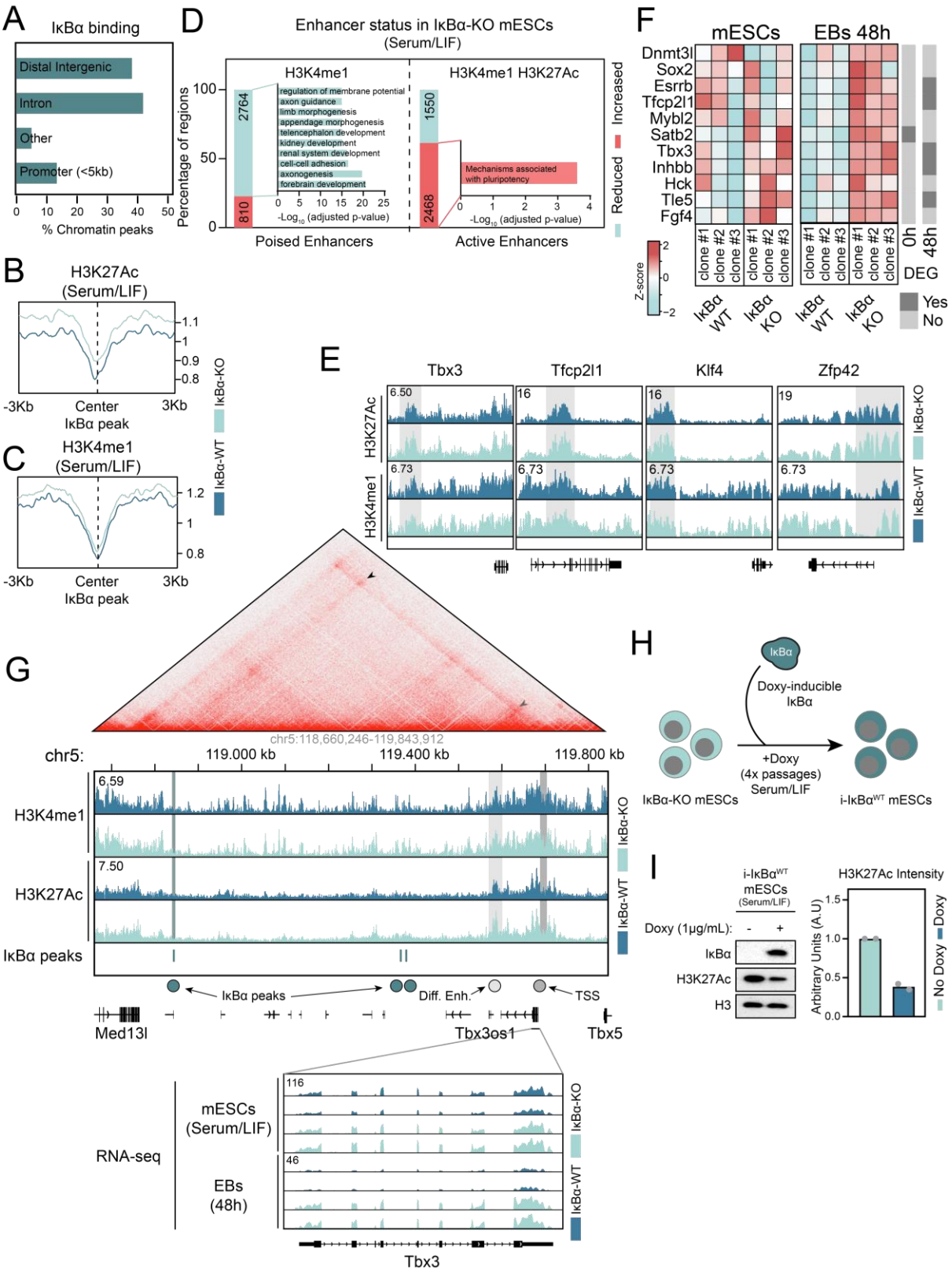

1023

1024

1025 **Figure 4. IκBα binds to enhancer regions to prevent their hyperactivation in the naïve**
1026 **pluripotency state. A.** Distribution of IκBα chromatin binding peaks. **B, C.** H3K27Ac (B) and

1027 H3K4me1 (C) distribution profiles in IκBα-WT vs IκBα-KO mESCs cultured in Serum/LIF in IκBα-
1028 bound chromatin regions. **D.** Number of regions with differential enhancer activity in IκBα-KO
1029 vs IκBα-WT mESCs cultured in Serum/LIF. Increased/Reduced activity for (left) poised
1030 enhancers based on the H3K4me1 differential binding and absence of H3K27ac overlapping
1031 peaks in IκBα-KO mESCs and, (right) active enhancers based on the differential binding of
1032 H3K27ac and presence of H3K4me1 overlapping peaks in IκBα-KO. Differential binding based
1033 on adjusted p-value <0.05 (FDR). Increased or reduced regions in IκBα-KO are distinguished
1034 by $\log_2$ Fold-change >0 or <0, respectively. Overrepresented WikiPathways for annotated
1035 genes with (left) reduced poised enhancers and (right) increased active enhancers in IκBα-KO
1036 mESCs are indicated (adjusted p-value < 0.05, FDR). **E.** Representative naïve pluripotency
1037 genes having an increase in active enhancer status in IκBα-KO mESCs. Shadowed regions
1038 highlight the differential levels of the histone mark. **F.** Expression of selected naïve
1039 pluripotency genes contained in TADs with active enhancer marks (H3K27Ac and H3K4me1)
1040 and IκBα binding in IκBα-WT and IκBα-KO mESCs and 48h EBs. **G.** (Upper panel) Contact map
1041 (Hi-C data from (Bonev et al. 2017)) of the TAD (chr5:118,785,000-119,707,000) which
1042 contains the Tbx3 locus. Arrows indicate the interaction between the IκBα-bound region and
1043 TSS of Tbx3 gene (upper arrow) or differential active enhancer (bottom arrow). (Center panel)
1044 Genome browser with H3K27Ac and H3K4me1 data in IκBα-WT and IκBα-KO mESCs.
1045 Shadowed areas indicate differential active enhancer (light gray), the TSS of the gene of
1046 interest (darker gray) or IκBα peaks (dark green). (Bottom panel) *Tbx3* expression (RNA-seq
1047 data) in IκBα-WT and IκBα-KO mESCs and 48h EBs from two independent clones. **H.** Schematic
1048 representation of IκBα reconstitution of IκBα-KO mESCs. **I.** Western blot analysis of H3K27Ac
1049 levels in i-IκBα^{WT} mESCs (left panel). Two independent experiments were performed to
1050 quantify H3K27Ac levels (right panel).

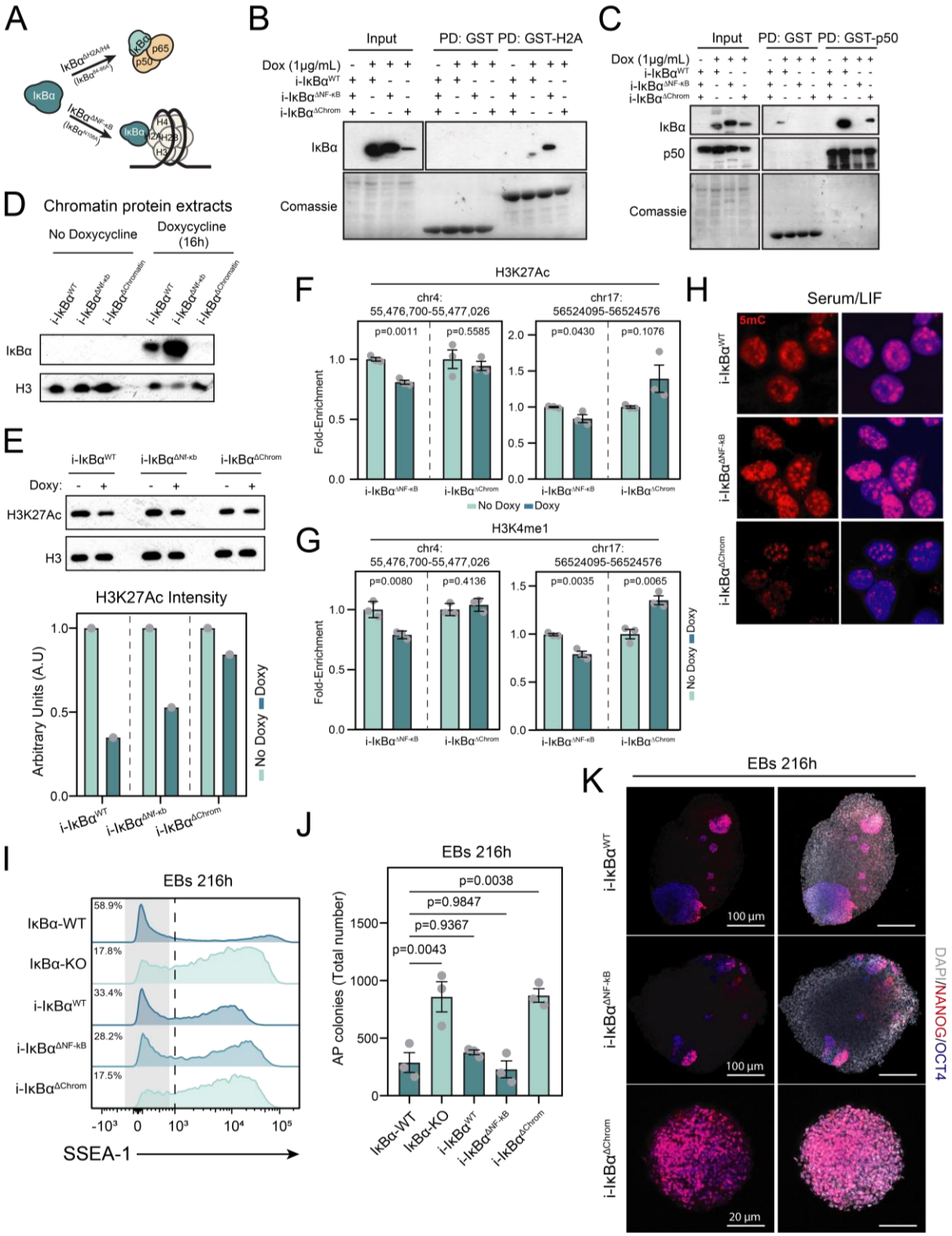

1051

1052 **Figure 5. IκBα safeguards enhancer hyperactivation in naïve pluripotency in an NF-κB-**
1053 **independent manner. A.** Schematic of chromatin-specific/NF-κB-deficient (IκBα$^{\Delta NF\text{-}\kappa B}$) or NF-
1054 κB-specific/chromatin-deficient (IκBα$^{\Delta Chrom}$) IκBα mutants. **B.** Pull-down of GST-H2A with cell
1055 lysates from different SOF IκBα mutant mESCs. **C.** Pull-down of GST-p50 with lysates from SOF
1056 IκBα mutant mESCs. **D.** Western blot analysis of chromatin protein extracts of doxycycline-

1057 inducible IκBα forms after 16h of doxycycline induction. **E.** Western blot analysis of H3K27Ac
1058 levels in i-IκBα^{WT}, i-IκBα$^{\Delta NF\text{-}\kappa B}$ and IκBα$^{\Delta Chrom}$ mESCs (upper panel). Quantification of H3K27Ac
1059 levels (bottom panel). **F, G.** ChIP-PCR of H3K27Ac (F) and H3K4me1 (G) marks within genomic
1060 regions bound by IκBα in i-IκBα$^{\Delta NF\text{-}\kappa B}$ and IκBα$^{\Delta Chrom}$ mESCs cultured in Serum/LIF. Unpaired
1061 two-sided t-test was performed. Bars indicate mean values and error bars refer to ± standard
1062 error of the mean (SEM). **H.** Representative immunofluorescence images of 5-methylcytosine
1063 (5mC) in i-IκBα$^{\Delta WT}$ (upper panel), i-IκBα$^{\Delta NF\text{-}\kappa B}$ (medium panel), IκBα$^{\Delta Chrom}$ (bottom panel) mESCs
1064 cultured in Serum/LIF. **I.** Flow cytometry of SSEA-1 at 216h EBs in i-IκBα^{WT}, i-IκBα$^{\Delta NF\text{-}\kappa B}$ and i-
1065 IκBα$^{\Delta Chrom}$ cells. **J.** Quantification of AP staining in 216h EBs upon reconstitution with the
1066 different IκBα forms. Each dot represents an independent experiment. One-way ANOVA was
1067 applied. Bars indicate mean values and error bars refer to ± SEM. **K.** Representative
1068 immunofluorescence for NANOG and OCT3/4 at 216h EBs in i-IκBα^{WT} (upper panel), i-IκBα$^{\Delta NF\text{-}\kappa B}$
1069 (medium panel) and i-IκBα$^{\Delta Chrom}$ (bottom panel) cells.

1070

1071

1072

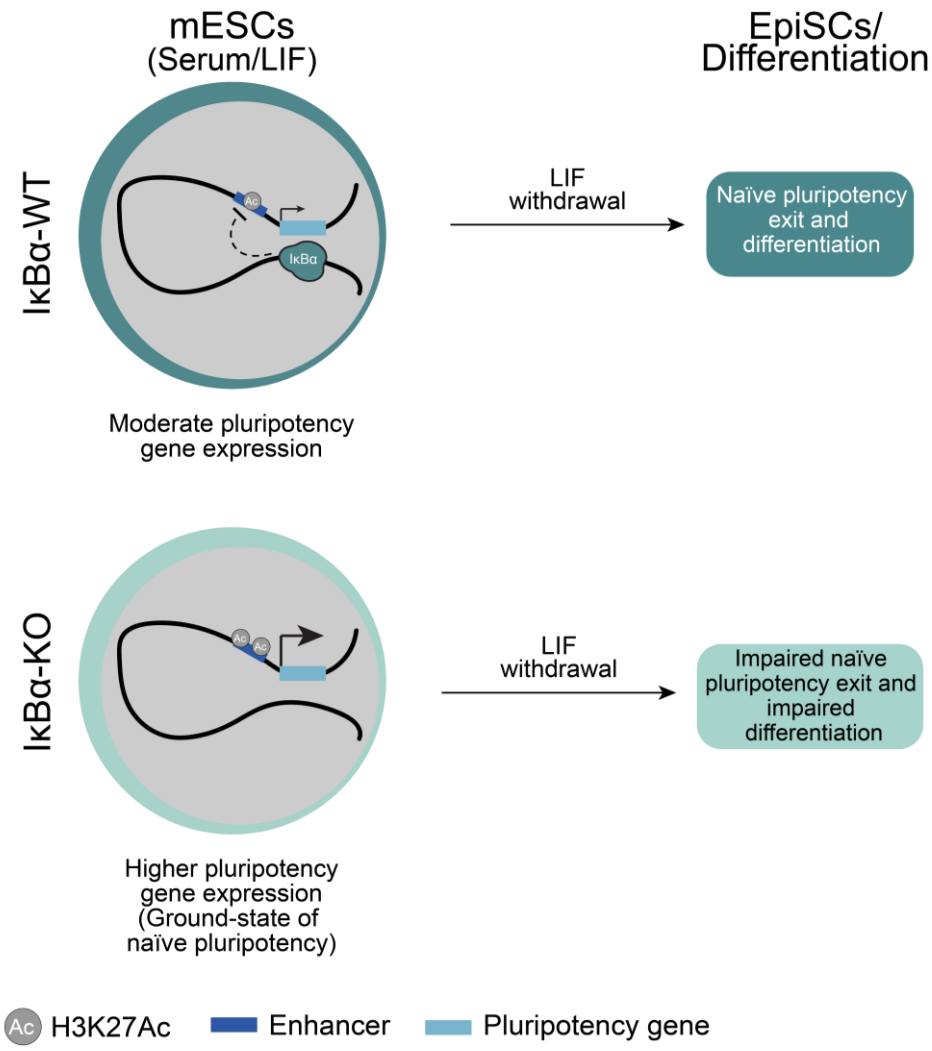

Figure 6. Proposed model: IκBα attenuates enhancer activity in the naïve-to-primed pluripotency transition. In mESCs cultured in Serum/LIF, IκBα binds to distal regions to maintain a moderate pluripotency gene expression by avoiding enhancer hyperactivation. This allows naïve pluripotency exit and differentiation upon LIF withdrawal. In the absence of IκBα, enhancer regions acquire a higher activation status, resulting in an aberrantly increased expression of pluripotency genes. This leads to an impaired pluripotency exit and differentiation.